The Astronomical Journal, 161:277 (22pp), 2021 June https://doi.org/10.3847/1538-3881/abf561

Calibration of the Hα Age–Activity Relation for M Dwarfs

Rocio Kiman[1,2,3], Jacqueline K. Faherty[2], Kelle L. Cruz[1,2,3,4], Jonathan Gagné[5,6], Ruth Angus[2,4,7], Sarah J. Schmidt[8], Andrew W. Mann[9], Daniella C. Bardalez Gagliuffi[2], and Emily Rice[1,2,10]
[1] Department of Physics, Graduate Center, City University of New York, 365 5th Avenue, New York, NY 10016, USA; rociokiman@gmail.com
[2] Department of Astrophysics, American Museum of Natural History, Central Park West at 79th Street, New York, NY 10024, USA
[3] Hunter College, City University of New York, 695 Park Avenue, New York, NY 10065, USA
[4] Center for Computational Astrophysics, Flatiron Institute, 162 5th Avenue, New York, NY 10010, USA
[5] Planétarium Rio Tinto Alcan, Espace pour la Vie, 4801 av. Pierre-de Coubertin, Montréal, Québec, Canada
[6] Institute for Research on Exoplanets, Université de Montréal, Département de Physique, C.P. 6128 Succ. Centre-ville, Montréal, QC H3C 3J7, Canada
[7] Department of Astronomy, Columbia University, 116th Street & Broadway, New York, NY 10027, USA
[8] Leibniz-Institute for Astrophysics Potsdam (AIP), An der Sternwarte 16, D-14482, Potsdam, Germany
[9] Department of Physics and Astronomy, The University of North Carolina at Chapel Hill, Chapel Hill, NC 27599, USA
[10] Macaulay Honors College, City University of New York, 35 W. 67th Street, New York, NY 10024, USA
Received 2020 August 14; revised 2021 March 29; accepted 2021 March 30; published 2021 May 21

Abstract

In this work, we calibrate the relationship between Hα emission and M dwarf ages. We compile a sample of 892 M dwarfs with Hα equivalent width (Hα EW) measurements from the literature that are either comoving with a white dwarf of known age (21 stars) or in a known young association (871 stars). In this sample we identify 7 M dwarfs that are new candidate members of known associations. By dividing the stars into active and inactive categories according to their Hα EW and spectral type (SpT), we find that the fraction of active dwarfs decreases with increasing age, and the form of the decline depends on SpT. Using the compiled sample of age calibrators, we find that Hα EW and fractional Hα luminosity ($L_{H\alpha}/L_{bol}$) decrease with increasing age. Hα EW for SpT $\leqslant$ M7 decreases gradually up until $\sim$1 Gyr. For older ages, we found only two early M dwarfs that are both inactive and seem to continue the gradual decrease. We also found 14 mid-type M dwarfs, out of which 11 are inactive and present a significant decrease in Hα EW, suggesting that the magnetic activity decreases rapidly after $\sim$1 Gyr. We fit $L_{H\alpha}/L_{bol}$ versus age with a broken power law and find an index of $-0.11^{+0.02}_{-0.01}$ for ages $\lesssim$776 Myr. The index becomes much steeper at older ages, but a lack of field age-calibrators ($\gg$1 Gyr) leaves this part of the relation far less constrained. Finally, from repeated independent measurements for the same stars, we find that 94% of them have a level of Hα EW variability $\leqslant$5 Å at young ages (<1 Gyr).

Unified Astronomy Thesaurus concepts: Low mass stars (2050); Astronomy data analysis (1858); Catalogs (205); Stellar activity (1580); Astrometric binary stars (79); Stellar evolution (1599)

Supporting material: machine-readable tables

1. Introduction

M dwarfs are the coolest and most abundant stars in the Milky Way (Gould et al. 1996; Bochanski et al. 2010). As the lifetime of M dwarfs is longer than the current age of the universe (e.g., Fagotto et al. 1994; Laughlin et al. 1997), those that we find throughout the Galaxy span a wide range of ages. Therefore M dwarfs are a rich stellar population for a statistical analysis of the Milky Way evolution, dynamics, and composition (e.g., Gizis et al. 2002; Bochanski et al. 2007, 2010; Faherty et al. 2009; Jones et al. 2011). In addition, M dwarfs are attractive targets for studying exoplanet populations because the occurrence of small rocky exoplanets is higher for M dwarfs than any other spectral type. Furthermore, it is easier to detect small planets around low-mass stars than around higher-mass stars due to the large reflex motion (e.g., Dressing & Charbonneau 2015; Mulders et al. 2015; Shields et al. 2016).

M dwarfs are intrinsically faint, especially toward later and cooler spectral types. Measuring their fundamental properties can therefore be challenging, even for the nearest ones (e.g., Ribas et al. 2017). However, several fundamental properties of M dwarfs have been studied extensively. For instance, using spectroscopy, photometry, and astrometry, effective temperature (e.g., Mann et al. 2015; Ness et al. 2015; Birky et al. 2020), radius (e.g., Kesseli et al. 2018), and luminosity (e.g., Reid & Cruz 2002), metallicity (e.g., Bochanski et al. 2013; Newton et al. 2014; Schmidt et al. 2016) and mass (e.g., Boyajian et al. 2012; Mann et al. 2019) measurements have been studied. Age, however, is one of the most difficult fundamental properties to evaluate, especially for M dwarfs (Soderblom 2010).

Current age-dating methods used for higher-mass stars cannot be applied to low-mass stars. Asteroseismology (e.g., Chaplin et al. 2014) is a common age-dating method for giant stars but cannot be applied to M dwarfs because their acoustic oscillations have extremely small amplitudes and short timescales (Rodríguez et al. 2016). Isochrones from stellar evolution models are not efficient either for estimating M dwarf ages due to the extremely slow and small changes in luminosity after 1 Gyr, making the isochrones very similar for older ages (Chabrier & Baraffe 1997). Furthermore, there are not sufficient empirical calibrations to validate isochrones for low-mass stars, especially at young ages. As a consequence, model isochrones still suffer from significant systematic errors that are unexplored and are inaccurate for precise age determinations (Baraffe et al. 2015). Empirical methods such as gyrochronology (e.g., Skumanich 1972; Barnes 2003, 2007; Angus et al. 2015; Van Saders et al. 2016) are either based on the Sun or are calibrated on higher-mass stars, and they do not

yield precise age estimates for M dwarfs (e.g., Angus et al. 2019). As currently available methods cannot be used to estimate M dwarf ages, empirically calibrated relations for age-related properties are needed.

Magnetic activity, age, and rotation period are known to be correlated for solar-type stars (e.g., Skumanich 1972; Barry 1988; Soderblom et al. 1991; Mamajek & Hillenbrand 2008). These stars have a radiative core and a convective envelope, and they do not rotate as a rigid body. As solar-type stars rotate, a magnetic dynamo is generated in between the two layers, which is responsible for their magnetic field (Parker 1955). Given that rotation and age are correlated for solar-type stars (e.g., Skumanich 1972; Barnes 2003, 2007; Angus et al. 2015; Van Saders et al. 2016), their magnetic activity is correlated with age as well. For the lowest-mass stars (spectral type >M3), the correlation between magnetic activity, age, and rotation is not well understood because these cool stars are fully convective (Chabrier & Baraffe 1997) and do not have an interface to produce a dynamo. However, previous studies of M dwarfs indicate that magnetic activity, rotation, and age are correlated (e.g., Eggen 1990; Fleming et al. 1995; Delfosse et al. 1998; Mohanty & Basri 2003; West et al. 2004, 2015; Reiners et al. 2012; Newton et al. 2017; Riedel et al. 2017; Angus et al. 2019; Kiman et al. 2019).

A well-studied magnetic activity indicator in M dwarfs is the Hα emission line (Hawley et al. 1996; West et al. 2008a, 2008b), which is generated by collisional excitations when magnetic field lines heat the dense chromosphere (Stauffer & Hartmann 1986). Therefore the Hα equivalent width (Hα EW) is an indirect measurement of the chromospheric magnetic activity of a star. The fact that M dwarf magnetic fields are driven by the stellar rotation means that the rotation-age correlation should translate into a Hα EW-age correlation (Newton et al. 2017). As a consequence, Hα EW could be used as an age indicator for M dwarfs. For low-mass stars, previous studies have confirmed that Hα emission is correlated with age by using kinematics as an age indicator (Gizis et al. 2002; West et al. 2008b; Kiman et al. 2019). West et al. (2008a) found a functional form for the age–activity relation from a sample of M dwarfs with Hα EW by modeling the relation between kinematics and age. However, to date, a study that empirically calibrates the age–activity relation for M dwarfs is still lacking.

A first necessary step for calibrating the Hα age–activity relation is to collect M dwarfs with known ages that are calculated with methods independent of the magnetic activity. The second data release of Gaia (Gaia Collaboration et al. 2016, 2018; Arenou et al. 2018; Lindegren et al. 2018) plays a key role in age-dating stars. The Gaia DR2 catalog contains $\sim$1.3 billion sources with a five-parameter astrometric solution: positions, parallaxes (π), and proper motions (μ) with unprecedented precision, down to a magnitude of $G = 21$. The parallax uncertainties (σ_π) are between 0.04 and 0.7 mas, and for proper motion (σ_μ), the uncertainties are between 0.06 and 1.2 mas yr^{-1}, depending on the magnitude of the star. With these high-quality measurements, Gaia made it possible to identify new stars that belong to age-calibrated moving groups and new associations (e.g., Faherty et al. 2018; Gagné & Faherty 2018; Kounkel & Covey 2019; Röser & Schilbach 2020), and new comoving pairs of stars (e.g., Oh et al. 2017; El-Badry & Rix 2018). Both young associations and comoving pairs can be sources for M-dwarf ages.

Moving groups and other coeval associations are ensembles of stars that are born from the same molecular cloud with common space velocities and a small spread of ages (Bell et al. 2015). As ages of the young associations are well calibrated down to a precision of a few million years (Soderblom 2010; Bell et al. 2015), the age of the association can be used to build a set of age-calibrated M dwarfs, if the stars can be identified as members.

Binary stars are born from the same molecular cloud at the same time (Bodenheimer 2011). Therefore we can calibrate the age of an M dwarf by constraining the age of a comover. For example, we can estimate a white dwarf's total age by adding the white dwarf cooling age and the main-sequence age of the progenitor star (Fouesneau et al. 2018). The white dwarf cooling age and mass are strongly constrained by cooling tracks from theoretical models (e.g., Bergeron et al. 1995, 2019; Fontaine et al. 2001). Using the mass of the white dwarf and the semiempirical initial-to-final mass relations (Cummings et al. 2018), we can estimate the mass of the progenitor star. Finally, with the mass of the progenitor star, we can calculate a main-sequence age, combined with the length of the pre- and post- (but pre-white dwarf) main-sequence stages (obtained with MESA models, Dotter 2016).

The aim of the present study is to calibrate the Hα age–activity relation for M dwarfs using a sample of age calibrators. We describe how we compiled a sample of M dwarfs with Hα EW measurements in the literature in Section 2. We show how we obtained the age calibrators from that sample by identifying M dwarfs that are comoving with a white dwarf with known age or members of known young associations in Section 3. The final table of age calibrators is described in Table 1. In Section 4 we describe the calculation of the fractional Hα luminosity from Hα EW for the age calibrators, which is a key parameter for calibrating the age–activity relation. In this section we also describe a search for known unresolved binaries that might bias our calibration of the age–activity relation. In Section 5 we show how we divided the sample of age calibrators into active or inactive objects according to their Hα EW measurement and photometry, and how we studied the relation between the active fraction and age for different spectral types. In Section 6 we discuss the relation between the Hα EW and fractional Hα luminosity with age and fit it using a Markov chain Monte Carlo (MCMC) algorithm. In Section 7 we compare our results for the age–activity relation with literature results for Hα, X-ray, and UV. Finally, in Section 8 we discuss our results and summarize our work and conclusions. All the code used in this work is available on Zenodo (Kiman 2021) and GitHub.[11]

2. Identifying M Dwarfs in the Literature with Hα Measurements

2.1. Compiling the Literature Search Sample

In order to empirically calibrate the age–activity relation for M dwarfs, we began by collecting M0-M9 dwarfs from the literature with a reported Hα EW. Kiman et al. (2019) compiled one of the largest published samples of M dwarfs with Hα EW, including measurements from West et al. (2011) and Schmidt et al. (2015). This sample contains 74,216 M dwarfs, 486 of which were removed because they have a spectroscopically

[11] https://github.com/rkiman/M-dwarfs-Age-Activity-Relation

Table 1
Columns in the Sample of Age Calibrators, Available as a FITS Table

Column name	Units	Description
ra	deg	Original R.A. from the source of the Hα measurement
dec	deg	Original Decl. from the source of the Hα measurement
spt		Spectral type
gaia_source_id	···	Unique Gaia source identifier (unique within DR2)
ra_gaia	deg	R.A. in Gaia DR2 epoch
dec_gaia	deg	Decl. in Gaia DR2 epoch
pmra	mas yr^{-1}	Proper motion in R.A. direction in Gaia DR2
pmra_error	mas yr^{-1}	Standard error of proper motion in R.A. direction in Gaia DR2
pmdec	mas yr^{-1}	Proper motion in decl. direction in Gaia DR2
pmdec_error	mas yr^{-1}	Standard error of proper motion in decl. direction in Gaia DR2
parallax	mas	Parallax in Gaia DR2
parallax_error	mas	Standard error of parallax in Gaia DR2
phot_g_mean_flux	electron s^{-1}	G-band mean flux
phot_g_mean_flux_error	electron s^{-1}	Error on G-band mean flux
phot_g_mean_mag	mag	G-band mean magnitude
phot_rp_mean_flux	electron s^{-1}	Integrated G_{RP} mean flux
phot_rp_mean_flux_error	electron s^{-1}	Error on the integrated G_{RP} mean flux
phot_rp_mean_mag	mag	Integrated GRP mean magnitude
phot_bp_mean_flux	electron s^{-1}	Integrated G_{BP} mean flux.
phot_bp_mean_flux_error	electron s^{-1}	Error on the integrated G_{BP} mean flux
phot_bp_mean_mag	mag	Integrated GBP mean magnitude
g_corr	mag	G magnitude corrected for extinction
rp_corr	mag	G_{RP} magnitude corrected for extinction
ewha	Å	Equivalent width Hα for the compatible literature search
ewha_error	Å	Equivalent width Hα error for the compatible literature search
ewha_all	Å	Equivalent width Hα for all the stars
ewha_error_all	Å	Equivalent width Hα error for all the stars
lhalbol	···	Fractional Hα luminosity
lhalbol_error	···	Fractional Hα luminosity error
age	yr	Age of the star
age_error_low	yr	Lower bound on the confidence interval of the estimated age
age_error_high	yr	Upper bound on the confidence interval of the estimated age
group_num	···	Number identifying the young association. 0 indicates a white dwarf companion
group_name	···	Young association to which the star belongs
star_index	···	Number indicating repeated stars. Same stars have the same number
source_num	···	Number indicating the source of the Hα measurement
source_ref	···	Source of the Hα measurement
potential_binary	···	1 if it is a potential binary, 0 if not.

(This table is available in its entirety in machine-readable form.)

identified but unresolved white dwarf companion (West et al. 2011; Schmidt et al. 2015), which could increase the magnetic activity of the star (Skinner et al. 2017). The remaining 73,730 M dwarfs from Kiman et al. (2019) make up the largest part of our literature search sample.

The M dwarfs in Kiman et al. (2019) are assumed to be primarily field stars. We complemented this sample with studies of M dwarfs in known star-forming regions, clusters, moving groups, or M dwarfs that are comoving with a white dwarf, as well as all the studies in the literature that have a measured Hα EW for cool dwarfs. All the studies we checked are listed or mentioned in Table 2. In total, we identified 89,270 stars from the literature (73,730 from Kiman et al. 2019 and 15,540 from other studies).[12] From the total number of stars in our sample, we found that 86,918 stars (97%) have photometric and astrometric information from Gaia DR2 (Gaia Collaboration et al. 2016, 2018). We applied the quality cuts described in Kiman et al. (2019) to select the best astrometric and photometric data from Gaia DR2 (the Sub Red sample). These cuts not only select best-quality photometry, parallaxes, and proper motions, but also remove possible unresolved binaries. We refer to Section 2.3 of Kiman et al. (2019) for more details. By applying these quality cuts, we were left with 27,201 M dwarfs (31%) in our literature search sample. In Section 3 we describe the cross-match with Gaia in more detail. We use the spectral type classification from the literature when available and estimate the spectral type for the remaining stars (6% of the sample) using their Gaia red color ($G - G_{RP}$) and the relation in Kiman et al. (2019). Although most of the studies we compiled were focused on M dwarfs, some contained higher-mass stars, mostly G and K dwarfs, which were removed with a cut in spectral type, keeping 25,720 M dwarfs ($\geqslant$M0).

From our literature search sample, 726 M dwarfs have between two and six measurements of Hα EW. We identified duplicates through a position search within a 2.″0 radius. These duplicated stars are indicated in the column star_index in Table 1. If two or more stars have the same number in this column, then they likely are the same star. In total, we found

[12] A catalog resulting from this literature search is available as a FITS table on Zenodo: doi:10.5281/zenodo.4659293.

Table 2
Age Calibrator Summary

References[a]	Spectral Resolution	*N* of M Dwarfs		OC[c]	Ages from	
		Total	Compatible[b]		Moving Group	White Dwarf
Kiman et al. (2019)	1800	73729	73729	0	46	21
LG11[d]	1000	2504	134	2	48	⋯
Jeffers et al. (2018)	62000, 48000, 40000	2133	2	2	22	⋯
Douglas et al. (2014)	3300, 4000	1906	50	1	264	⋯
Lepine et al. (2013)	2000,4000	1577	1	2	4	⋯
Riaz et al. (2006)	1750	1098	4	2	65	⋯
Ansdell et al. (2015)	1000, 1200	794	35	2	31	⋯
Gaidos et al. (2014)	1200	582	59	2	2	⋯
Fang et al. (2018)	1800	561	1	1	159	⋯
Newton et al. (2017)	3000	456	14	2	2	⋯
Terrien et al. (2015)	2000	351	13	2	2	⋯
Reid et al. (1995)	2000	343	4	2	1	⋯
Schneider et al. (2019)	32000	336	10	2	26	⋯
Bouy & Martín (2009)	Multiple	227	1	2	135	⋯
Kraus et al. (2014)	35000	205	2	2	88	⋯
Shkolnik et al. (2009)	60000	184	7	2	9	⋯
Alonso-Floriano et al. (2015)	1500	179	8	2	3	⋯
Slesnick et al. (2008)	1250	145	69	2	23	⋯
Malo et al. (2014a)	1750	120	1	2	45	⋯
Torres et al. (2006)	50000, 9000	114	2	2	18	⋯
Shkolnik et al. (2017)	35000, 58000	106	3	2	24	⋯
Elliott et al. (2016)	85000, 48000	83	2	2	3	⋯
Reiners & Basri (2010)	31000	73	2	1	2	⋯
Slesnick et al. (2006)	1250	65	19	2	18	⋯
Jayawardhana et al. (2006)	60000	52	1	2	20	⋯
Riedel et al. (2014)	Multiple	50	3	2	5	⋯
Hawley et al. (1996)	2000	31	1	2	1	⋯
Song et al. (2003)	24000	25	1	2	3	⋯
Rodriguez et al. (2014)	3000, 7000	23	12	2	12	⋯

Notes.
[a] Compatible catalogs without age calibrators: Gizis et al. (2002), Mochnacki et al. (2002), Reid & Cruz (2002), West et al. (2011), Song et al. (2004), Lyo et al. (2004). Catalogs with overlap but not compatibles: Mohanty et al. (2005), Shkolnik et al. (2011), Lawson et al. (2002). Catalogs without overlap: Frasca et al. (2018), Bayo et al. (2012), Reid et al. (2007), Cruz & Reid (2002), Feigelson et al. (2003), Gizis et al. (2000), Gizis & Reid (1997), Murphy et al. (2010), Phan-Bao & Bessell (2006), Bochanski et al. (2005), Mohanty & Basri (2003), Reiners & Basri (2007, 2008), Lépine et al. (2003, 2009), Martin & Kun (1996), Ivanov et al. (2015), Stauffer et al. (1997), Tinney & Reid (1998). Other catalogs checked: Lodieu et al. (2005).
[b] Compatible with Kiman et al. (2019).
[c] Order of compatibility. Order 1 is compatible with Kiman et al. (2019). Order 2 is compatible with at least one order 1 catalog.
[d] Lepine et al. (2013) and Gaidos et al. (2014) with additional data observed in an identical manner.

that our literature search sample has 24,330 unique M dwarfs with good data from Gaia DR2 and Hα EW measurements.

2.2. Identifying Compatible Hα Measurements from the Literature

The Hα EW is calculated by dividing the flux below the emission line of Hα by the flux of the continuum. Both sources of Hα EW for Kiman et al. (2019; West et al. 2011; Schmidt et al. 2015) used the same definition for the emission line: 6557.61–6571.61 Å, and the surrounding continuum: 6530–6555 and 6575–6600 Å. Both West et al. (2011) and Schmidt et al. (2015) measured the Hα EW from spectra with $R \sim 1800$ resolution. Our literature search sample, however, contains objects with measurements of Hα EW from different spectral resolutions (shown in Table 2) that were calculated with slightly different definitions of the line and the continuum. This diversity of approaches and results could cause inconsistencies in our analysis. To account for the differences between Hα EW measurements, we followed a procedure similar to the one described in Newton et al. (2017). We only used the Hα EW from catalogs that were compatible with the Kiman et al. (2019) sample, as that is the largest component of our literature search sample (see Section 2.1). We considered a given catalog compatible if it had at least one star in common and if at least 90% of the stars in common had a difference in Hα EW smaller than 3 Å ($|\Delta \mathrm{H}\alpha\ \mathrm{EW}| < 3$ Å) with the measurement in Kiman et al. (2019). We chose 3 Å as the limit because this is the typical Hα variability for M4 − M5 identified by Lee et al. (2010) in a spectroscopic survey of 43 M dwarfs in the range M3.5 − M8.5. This cut assumes that 90% of the M dwarfs have small variability. We note that this might bias against variable >M5 dwarfs because variability increases for later types (Lee et al. 2010).

We defined the criterion described above as first-order compatibility, and it is indicated with a 1 in the column "OC" of Table 2. We could only find three catalogs from the literature search that had overlapping stars with Kiman et al. (2019): Douglas et al. (2014), Fang et al. (2018), and Reiners & Basri (2010). Therefore we decided to iterate upon our method and search for further studies compatible with these three catalogs to increase the number of stars we consider compatible. We

Table 3
Short Sample of Hα EW Outliers that Are Possibly Accreting According to the Criterion from White & Basri (2003)

2MASS Name	SpT	Hα EW	ΔHα EW[a]
J16075567−2443267	M5.5	47.3 ± 0.1	27.3
J05353004+0959255	M5.6	22.82 ± 0.62	2.82
J05334992+0950367	M2.3	14.01 ± 0.51	4.01
J12350424−4136385	M2.5	13.6 ± 0.2	3.6
J02591904−5122341	M5.4	32.11 ± 0.1	12.11
J16104996−2212515	M5.5	23 ± 0.1	3
J04480085+1439583	M5.0	73.6 ± 0.1	53.6
J04262939+2624137	M6.0	97.7 ± 9.8	57.7
J05340393+0952122	M2.2	30.2 ± 1.14	20.2
J12071089−3230537	M4.3	114.8 ± 0.5	94.8

Notes. The full sample can be found online.
[a] Delta above the Hα EW limit.

(This table is available in its entirety in machine-readable form.)

repeated the procedure described above to find what we defined as second-order compatibility catalogs. These second-order compatibility catalogs do not have stars in common with Kiman et al. (2019), but they do have stars in common with at least one of the order 1 catalogs.

All in all, we found 24,202 unique M dwarfs (99.6% of the sample) with Hα EW measurements that were either in Kiman et al. (2019, order 0) or first- or second-order compatible, meaning that we can use them together to calibrate the age–activity relation. We excluded the 128 remaining M dwarfs from our analysis.

2.3. Removing Potentially Accreting M Dwarfs

To characterize the age–activity relation, we are interested in chromospheric Hα emission, but this spectral line could in some systems result from accretion. To distinguish between the two types of emission, we used an empirical criterion that depends on the star's Hα EW and spectral type, developed by White & Basri (2003) based on a sample of low-mass T Tauri stars. They proposed that a T Tauri star is classical, meaning accreting, if $H\alpha\,EW \geqslant 10\,\AA$ for K7 − M2.5 stars, $H\alpha\,EW \geqslant 20\,\AA$ for M3 − M5.5, and $H\alpha\,EW \geqslant 40\,\AA$ for M6 − M7.5 stars.

Based on the White & Basri (2003) criterion, we removed 45 stars that are Hα outliers from our analysis because they are possibly accreting. It should also be noted that by using only Hα EW to discard possible accretors, we are also removing Hα EW outliers such as nonaccreting stars whose measurement of Hα was taken during a flare. In Table 3 we list the Hα EW outliers that are possibly accreting, identified in this study with their 2MASS name, spectral type, the Hα EW, and ΔHα EW above the limit defined by White & Basri (2003). Given that the criteria only extend to M7.5, we did not remove any later spectral types according to their Hα EW. Therefore we are likely to have some contamination from accreting later spectral types.

3. Identifying M Dwarfs in Young Associations and Comoving with White Dwarfs

3.1. Identifying Young Association Members

As mentioned in Section 2.1, we complemented Kiman et al. (2019) with M dwarfs that were classified as members of young associations by previous studies and/or had Hα EW measurements. However, most of these studies were completed prior to the release of Gaia DR2, which provided kinematics of an unprecedented quality.

In light of the new astrometric improvement of the Gaia DR2 survey, we decided to re-assess the likelihood of membership for each source and/or identify new members. To obtain proper motions and parallaxes for our literature search sample, we used TOPCAT (Taylor 2005) and a 2″ radius for a match with Gaia DR2 objects. We found 97% (86,918 out of the original 89,270 sources) of our literature search sample in Gaia DR2. As mentioned in Section 2.1, we applied the quality cuts described in Kiman et al. (2019) to obtain the best astrometric and photometric data and to remove potential binaries, and we were left with 27,201 M dwarfs. To look for mismatches, we used the 726 M dwarfs in our sample with duplicated measurements of Hα EW (see Section 2.1) and compared their Gaia source id. All the duplicated stars had the same Gaia source id, except for 6 stars that we think are potentially unresolved M dwarf binaries because after visually inspecting them, we found that there was only one star with two Gaia sources in the image. These 6 stars were removed from our analysis.

To confirm or identify members of young associations from our literature search sample, we used the BANYAN Σ Bayesian membership classification algorithm (Gagné et al. 2018).[13] BANYAN Σ models young associations with a multivariate Gaussian density. This Gaussian has a total of six dimensions: three galactic positions (XYZ), and three space velocities (UVW). BANYAN Σ also models the galactic field within 300 pc by combining 10 multivariate Gaussians. To calculate the probability of a star belonging to a young association or the field, BANYAN Σ compares observables such as position and proper motion to the multivariate Gaussian model in a Bayesian classification likelihood, and marginalizes over radial velocities and distances when they are not available. The marginalization integrals are solved with an analytical solution, making the code more precise and efficient. In total, 27 associations are modeled in BANYAN Σ within 150 pc. A summary of the associations in BANYAN Σ is provided in Table 4.

Using BANYAN Σ, we calculated the probability that any given M dwarf belongs to a known association according to its position, proper motion, parallax, and radial velocity when available from Gaia DR2. We used this code to analyze the 24,166 single, compatible, not accreting stars in our sample (see Section 2).

To remove as many false positives as possible without loosing true positives, we used a 90% cutoff in the membership probability output by BANYAN Σ, as suggested by Gagné et al. (2018). In total, we found 871 M dwarfs, which yielded a 90% probability in a known young association. The remaining 23,274 stars were rejected as young association members by our cut and/or have a high probability (>90%) to be field stars according to BANYAN. In addition, 21 objects were removed because they were rejected as young association members by Gagné et al. (2018). These objects were rejected mostly

[13] The IDL version is available at https://github.com/jgagneastro/banyan_sigma_idl. The Python version is also available at https://github.com/jgagneastro/banyan_sigma, and the web portal is available at http://www.exoplanetes.umontreal.ca/banyan/banyansigma.php.

Table 4
Young Associations in Banyan Σ (Gagné et al. 2018) and Summary of M Dwarfs in Young Associations Used in This Work

Association	Short name	Age (Myr)	Age Refernces[a]	Total Members[b]	New Members
Taurus	TAU	1.5 ± 0.5	1	3	⋯
ρ Ophiuchi	ROPH	<2	2	⋯	⋯
ϵ Chamaeleontis	EPSC	3.7 ± 4.6	3	9	1
Corona Australis	CRA	4–5	4	⋯	⋯
TW Hya	TWA	10.0 ± 3.0	5	10	⋯
Upper Scorpius	USCO	10.0 ± 3.0	6	167	1
118 Tau	118TAU	$\sim$10	7	⋯	⋯
Upper CrA	UCRA	$\sim$10	8	1	⋯
η Chamaeleontis	ETAC	11.0 ± 3.0	5	1	⋯
Lower Centaurus Crux	LCC	15.0 ± 3.0	6	20	1
Upper Centaurus Lupus	UCL	16.0 ± 2.0	6	4	2
32 Orionis	THOR	22^{+4}_{-3}	5	⋯	⋯
β Pictoris	βPMG	24.0 ± 3.0	5	54	1
Octans	OCT	35.0 ± 5.0	3	1	⋯
Argus	ARG	40–50	9	1	⋯
Columba	COL	42.0 ± 6.0	5	12	⋯
Carina	CAR	45.0 ± 11.0	5	6	⋯
Tucana–Horologium association	THA	45.0 ± 4.0	5	97	⋯
Platais 8	PL8	$\sim$60	10	⋯	⋯
Pleiades cluster	PLE	112 ± 5	11	106	⋯
AB Doradus	ABDMG	149.0 ± 51.0	5	36	1
Carina-Near	CARN	200.0 ± 50.0	12	3	⋯
core of the Ursa Major cluster	UMA	414.0 ± 23.0	13	1	⋯
χ^1 For	XFOR	$\sim$500	14	⋯	⋯
Coma Berenices	CBER	562.0 ± 98.0	15	9	⋯
Praesepe cluster[c]	PRA	650.0 ± 50.0	16	251	⋯
Hyades cluster	HYA	750.0 ± 100.0	17	79	⋯

Notes.
[a] (1) Kenyon & Hartmann (1995), (2)Wilking et al. (2008), (3) Murphy & Lawson (2015), (4) Gennaro et al. (2012), (5) Bell et al. (2015), (6) Pecaut & Mamajek (2016), (7) Mamajek (2016), (8) Gagné et al. (2018), (9) Zuckerman (2019), (10) Platais et al. (1998), (11) Dahm (2015), (12) Zuckerman et al. (2006), (13) Jones et al. (2015), (14) Pöhnl & Paunzen (2010), (15) Silaj & Landstreet (2014), (16) Douglas et al. (2019); Gao (2019), (17)Brandt & Huang (2015).
[b] Total number of stars with Hα compatible (see Section 2.2).
[c] Praesepe is not included in the current public version of Banyan Σ (v1.2, 2018 September 6).

because their literature radial velocity was inconsistent with that of the group.

Based on experience with kinematics and lithium abundances, we expect an average contamination from false members below 10% (Gagné et al. 2018). In Appendix A we show the color–magnitude diagrams for each of the young associations with all of the objects used in this study as members. We concluded that we cannot discard any objects with the color–magnitude diagrams. The distribution of members per young association is shown in Figure 1 and Table 4. We found that Praesepe ($\sim$650 Myr, 251 sources) had the highest yield of objects from our sample, followed by Upper Scorpious ($\sim$10 Myr, 167 sources), the Pleiades cluster ($\sim$112 Myr, 106 sources), and Tucana–Horologium ($\sim$45 Myr, 97 sources). Therefore we compiled a significant number of stars covering a range of ages that allows us to calibrate the age–activity relation for ages $<$1Gyr.

From the 871 young association members in this work, we found that 708 have the same original membership assigned in the literature, 17 had their moving group membership revised, and 167 were not identified as members in our literature search. From the 184 "new" candidate members or members that changed their membership, 2 were rejected as members using radial velocities from the literature, and 175 have previously been identified as young association members by studies not collected in this work, i.e., studies where Hα measurements were not used (Röser et al. 2011; Gagné & Faherty 2018; Gagné et al. 2018; Galli et al. 2018; Goldman et al. 2018; Luhman et al. 2018;

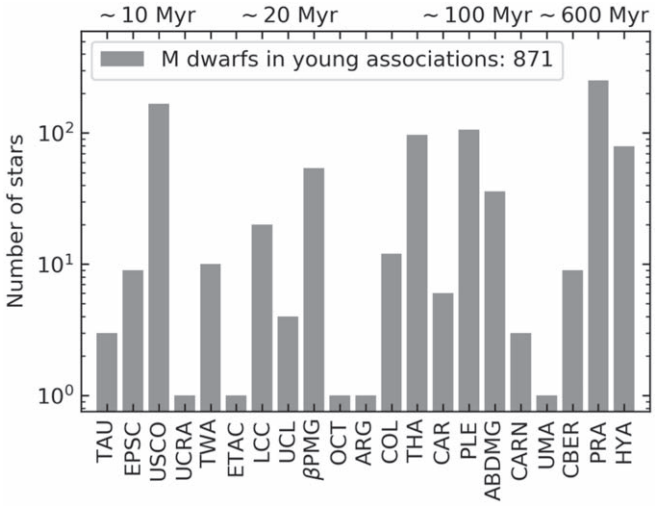

Figure 1. Membership distribution for M dwarfs in our sample, with young associations ordered by age. We include a reference at the top of the figure for the age of each association. Repeated measurements are not included in the total number of stars per association. References for each association are listed in Table 4.

Table 5
New Candidate Members of Known Young Associations Found in This Study

2MASS Name	SpT	Young Association	Source
J06511842−2154268	M1.5	ABDMG	Riaz et al. (2006)
J03273084+2212382	M4.5	BPMG	Jeffers et al. (2018)
J12323103−7255068	M3.5	EPSC	Riaz et al. (2006)
J12554838−5133385	M2.0	LCC	Riaz et al. (2006)
J15264071−6110559	M3.0	UCL	Riaz et al. (2006)
J16544682−3502540	M4.0	UCL	Riaz et al. (2006)
J16040453−2346377	M4.0	USCO	Slesnick et al. (2006)

Rebull et al. 2018). The remaining 7 M dwarfs are new candidate members of the young associations identified in this study. In particular, 2MASS J12323103-7255068 was called a member of LCC by Goldman et al. (2018), which we revised to be a member of EPSC. These stars are summarized in Table 4 and listed in Table 5.

As a further check on the membership probabilities for the new candidate members (or those that changed membership group), we compared their position in the Gaia color–magnitude diagram to that of empirical sequences based on bona fide members of young association of different ages (Gagné et al. 2020), and members of each association (Gagné et al. 2018). To compare an individual star's position in a color–magnitude diagram, it is important to evaluate the extinction due to interstellar dust. We used the extinction maps of STructuring by Inversion of the Local InterStellar Medium (STILISM; Lallement et al. 2014; Capitanio et al. 2017; Lallement et al. 2018)[14] and the method of Gagné et al. (2020) to calculate dereddened Gaia DR2 G- and $G_{\rm RP}$-band magnitudes. In summary, a template spectrum of the appropriate spectral type is used to calculate the effect of a typical interstellar dust extinction curve on the full Gaia bandpasses and stellar spectra, a step that is required because the Gaia bandpasses are particularly wide. Interstellar extinction will thus typically move M dwarfs down along isochrones (redder colors and fainter magnitudes) in a Gaia absolute G versus $G-G_{\rm RP}$ color–magnitude diagram, but it will move the high-mass stars horizontally to redder colors, and across distinct isochrones. The position in the color–magnitude diagram of our new candidate members is shown in Figure 2 and is compared to empirical sequences based on bona fide members of young associations of different ages (Gagné et al. 2020) and members of Upper Scorpius, Lower Centaurus Crux, Upper Centaurus Lupus, βPictoris, and AB Doradus (Gagné et al. 2018). We performed a visual inspection of all the high-probability members, and found that all the stars lie around the corresponding age sequences and/or within the scatter of the groups. This comparison corroborates their BANYAN Σ membership classifications when the scatter of the group is taken into account. However, more study is needed before they are confirmed as members. The summary of the catalogs we used to compile all these M -dwarf age calibrators with Hα EW measurements with a >90% probability of membership in a young association is given in Table 2.

3.2. Identifying and Age-dating Comovers with White Dwarfs

With BANYAN Σ, we can cover age calibrators up to ∼750 Myr. For older ages we turned to white dwarfs as chronometers to identify older age calibrators. White dwarf cooling models and model atmospheres are robustly developed to estimate precise and reliable cooling ages and masses (Fontaine et al. 2001). These models can be used to calculate total ages with a 10%–20% precision (Fouesneau et al. 2018) and as old as 12 Gyr (Cummings et al. 2018). Using comoving white dwarf systems as age calibrators therefore greatly expands the range used for grounding the age–activity relation.

The summary of the catalogs in which we found M dwarfs with a white dwarf comover that served as age calibrators is given in Table 2. To find M dwarfs that are comoving with white dwarfs, we cross-matched our literature search sample with the white dwarf catalog of Gentile Fusillo et al. (2019) using a 10′ radius. Gentile Fusillo et al. (2019) used a catalog of spectroscopically identified white dwarfs from the Sloan Digital Sky Survey (York et al. 2000) to define cuts to select 486,641 white dwarfs from the Gaia DR2 color–magnitude diagram. In our study we only used the 260,000 high-confidence white dwarf candidates ($P_{\rm WD}>0.75$), as suggested by Gentile Fusillo et al. (2019).

To find M dwarfs that are comoving with a white dwarf, we used the 23,274 sources that had good Gaia data, but were rejected as young association members and/or have a high probability (>90%) to be field stars according to BANYAN Σ (Section 3.1). We did not look for white dwarfs that are comoving with M dwarf members of young associations because the age of the moving group is better constrained than the estimation of the white dwarf age (see Section 1). Additionally, companion searches within young associations based solely on kinematics produces many false positives due to their high probability of chance alignment.

We considered an M dwarf and a white dwarf to be comoving if

1. $\pi_{\rm wd}/\sigma_{\pi,{\rm wd}}>4$
2. $\pi_m/\sigma_{\pi,m}>10$
3. $|\mu_{\alpha,{\rm wd}}-\mu_{\alpha,m}|<3\times(\sigma_{\mu_{\alpha,{\rm wd}}}+\sigma_{\mu_{\alpha,m}})$
4. $|\mu_{\delta,{\rm wd}}-\mu_{\delta,m}|<3\times(\sigma_{\mu_{\delta,{\rm wd}}}+\sigma_{\mu_{\delta,m}})$
5. $|\pi_{\rm wd}-\pi_m|<3\times(\sigma_{\pi,{\rm wd}}+\sigma_{\pi,m})$.

The cut on the signal-to-noise ratio for the white dwarf parallax ($\pi_{\rm wd}/\sigma_{\pi,{\rm wd}}$) is lower than for M dwarfs, as suggested by Gentile Fusillo et al. (2019), and the signal-to-noise ratio for M dwarfs ($\pi_m/\sigma_{\pi,m}$) follows the suggestions by Lindegren et al. (2018). For both components of the proper motion (μ_α and μ_δ) and the parallax (π), we required that the difference between the value for the white dwarf and the M dwarf in a pair was smaller than 3σ, where σ is the sum of the errors in each parameter. In total, we found 61 pairs with these criteria.

To remove false-positive companions, we calculated the probability of chance alignment for each M dwarf by reassigning the0 proper motions of all the white dwarfs in Gentile Fusillo et al. (2019) and repeating the search for comovers with the criteria described above, $N=1000$ times. We then calculated the probability of chance alignment for each M dwarf as $n_{\rm rand}/N$, where $n_{\rm rand}$ is the number of random comovers, and required it to be smaller than 0.01 to include a pair in our analysis. By adding this cut on probability of chance alignment, we remove pairs with several close-by white dwarfs, which makes a random match more likely. Out of the 61 pairs found, 22 had a probability of chance alignment higher than 0.01.

To calibrate the age–activity relation, wide white dwarf-M dwarf pairs are key to assuming that both components

[14] Available at https://stilism.obspm.fr.

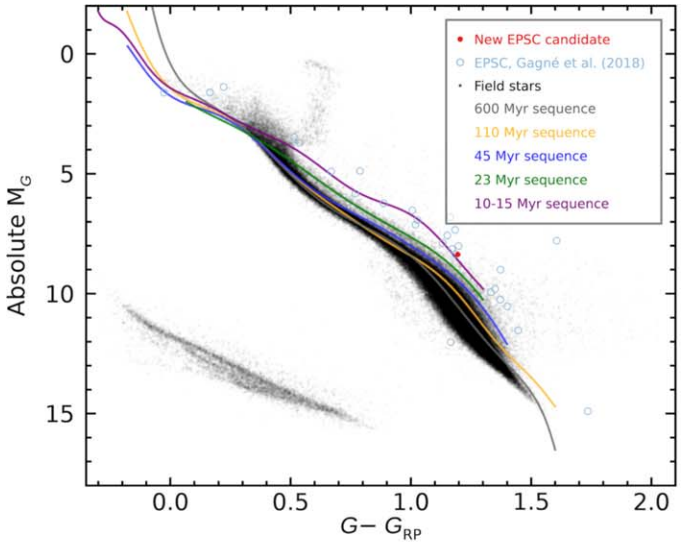

(a) ϵ Chamaeleontis, 3.7 ± 4.6 Myr.

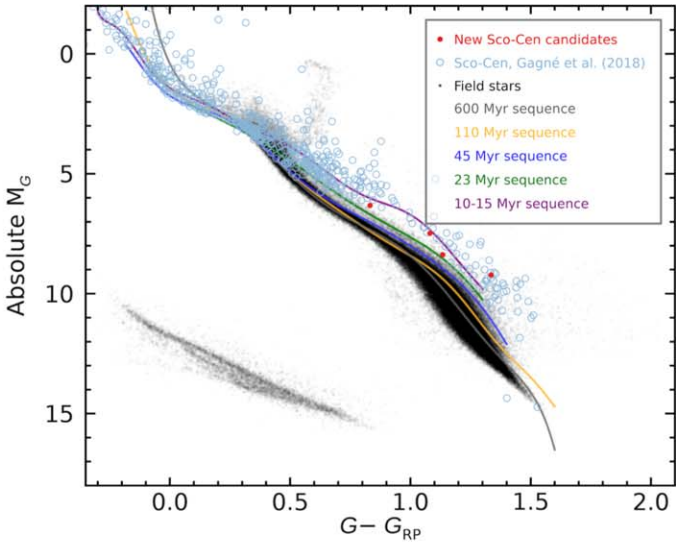

(b) Upper Scorpius, 10.0 ± 3.0 Myr, Lower Centaurus Crux, 15.0 ± 3.0 Myr and Upper Centaurus Lupus, 16.0 ± 2.0 Myr.

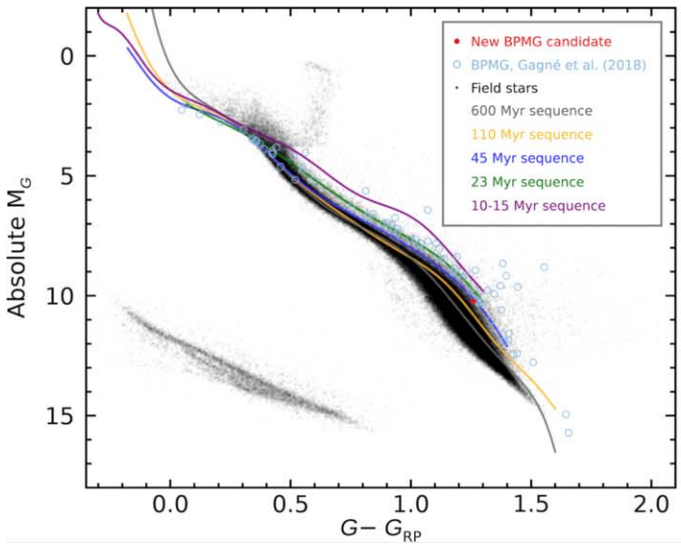

(c) β Pictoris, 24.0 ± 3.0 Myr.

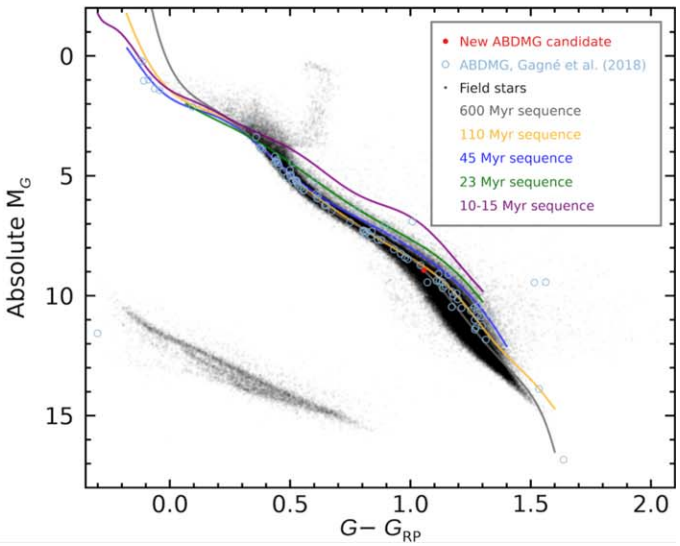

(d) AB Doradus, 149.0 ± 51.0 Myr.

Figure 2. Color–magnitude diagrams to check membership of the newly identified candidate members for each young association (see Table 5). New candidate members are shown as a red points on top of a field sample from Gaia DR2 in black. We include empirical sequences based on bona fide members of young associations of several ages (Gagné et al. 2020) and the members of the groups as light blue empty circles (Gagné et al. 2018). References for each young association are given in Table 4. The color–magnitude diagrams do not discard the new candidate members, but more study is needed before they are confirmed as members.

evolved as single stars without interacting. We estimated the physical separation between the pairs as $a = 1.22\theta \times D$, where a is the separation in au, θ is the angular separation, and D is the distance in parsecs. We found that the closest pair is separated by $\sim$500 au, therefore we can assume that the two stars in each pair evolved independently (Dhital et al. 2015; Skinner et al. 2017).

Once we identified the 39 M dwarf-white dwarf pairs, we used the open-source Python package available online, `wdwarfdate` (R. Kiman et al. 2021, in preparation)[15], to estimate their age. `wdwarfdate` estimates ages of white dwarfs in a Bayesian framework from an effective temperature and a surface gravity. Twenty-one of the total number of pairs had effective temperature and surface gravity from Gentile Fusillo et al. (2019) and were in the ranges in which the models we use are valid. Using this information and cooling models (Bergeron et al. 1995, 2011; Fontaine et al. 2001; Holberg & Bergeron 2006; Kowalski & Saumon 2006; Tremblay et al. 2011; Blouin et al. 2018)[16], we obtained the cooling ages and the masses of the white dwarfs. With a semiempirical initial-final mass relation (Cummings et al. 2018) and the masses of the white dwarfs, we obtained the masses of the progenitor stars, which were used with the MESA Isochrones (Paxton et al. 2011, 2013, 2015, 2018; Choi et al. 2016; Dotter 2016) to

[15] https://wdwarfdate.readthedocs.io/en/latest/

[16] http://www.astro.umontreal.ca/~bergeron/CoolingModels/

Table 6
Ages for the White Dwarfs that Are Comoving with an M Dwarf

Gaia Source Id		Total Age (Gyr)
M Dwarf	White Dwarf	
2543566734628019712	2543472279707400320	$3.05^{+3.61}_{-1.15}$
2544030286155342080	2544024582438777088	$1.41^{+3.5}_{-0.79}$
2536947571549610368	2536960490812885760	$2.57^{+3.65}_{-1.04}$
2536695439789556352	2536705752006690304	$1.94^{+3.58}_{-1.03}$
3264871552432918528	3264871552432918784	$1.71^{+3.58}_{-1.05}$
676167219784728576	676167215489980800	$2.57^{+4.31}_{-1.33}$
703747197659174528	703753485491279488	$0.64^{+1.84}_{-0.31}$
636424547365777152	636417842920590208	$2.56^{+3.36}_{-0.95}$
799122031706484736	799133954536821248	$3.04^{+2.97}_{-1.08}$
793350660811961984	793351038769083776	$2.31^{+3.33}_{-0.93}$
743097619303531776	743097619303531904	$2.91^{+4.42}_{-1.87}$
4030722598505336192	4030722594210006784	$3.53^{+3.5}_{-1.57}$
3898427744542897152	3898427744542897408	$1.67^{+2.12}_{-0.48}$
4006695825601458816	4006671533266385792	$5.2^{+3.18}_{-1.81}$
3928724924885805568	3928724512568932992	$1.27^{+2.75}_{-0.67}$
1465169548332089472	1465169548332089600	$1.94^{+4.09}_{-1.17}$
1610798793983536384	1610800271452287488	$2.46^{+4.15}_{-1.55}$
4424639574212380800	4424639368053787776	$3.66^{+2.37}_{-1.03}$
1321738561431758592	1321738565727229184	$4.87^{+4.04}_{-2.06}$
1328907068007155072	1328909232670299904	$4.61^{+3.08}_{-1.68}$
4467448891937012992	4467448853280423296	$4.35^{+2.67}_{-1.23}$

determine the ages of the progenitors. By adding the cooling ages and the ages of the progenitors, we obtained the total ages. In this process we assumed that all the white dwarfs are DA, meaning that they have a hydrogen-dominated atmosphere, which is a good approximation given that most of the white dwarfs in the galaxy are DA. We also assumed solar metallicity and $v/vcrit = 0$ for the progenitors. We refer to R. Kiman et al. (2021, in preparation) for more details about the calculation of the ages of the white dwarfs that are comoving with an M dwarf. The results are shown in Table 6, where we provide the Gaia DR2 `source_id` for the M dwarf and the white dwarf in each comoving pair and the estimated total age. Uncertainties are calculated as the 84th percentile minus the median as high error and the median minus the 16th percentile as low error.

4. Measurements and Unresolved Binaries

4.1. Calculating $L_{H\alpha}/L_{bol}$ for the Age calibrators

The activity strength of M dwarfs is usually quantified with the ratio of the Hα luminosity to the bolometric luminosity $L_{\rm H\alpha}/L_{\rm bol}$ (Hawley et al. 1996; West et al. 2008b; Schmidt et al. 2015). Using this fractional Hα luminosity removes the dependence on the continuum of the Hα EW and facilitates the comparison of stars of different effective temperatures. $L_{\rm H\alpha}/L_{\rm bol}$ was calculated using the "χ" factor (e.g., Walkowicz et al. 2004), where

$$L_{\rm H\alpha}/L_{\rm bol} = \chi({\rm SpT}) \times {\rm H}\alpha\ {\rm EW}.$$

The χ values were empirically calibrated as a function of spectral type using M0 – M9 from the Praesepe and Hyades clusters by Douglas et al. (2014). Given that at the ages of these clusters (~700 Myr), M dwarfs have almost completely converged to the main sequence, we can assume that the χ values are valid for field dwarfs. However, the χ values may vary for younger stars and/or stars with different metallicities. In our analysis, we assume that the difference in χ values for younger stars or different metallicities is not significant. Note that these might be strong assumptions, but to our knowledge, no better suited calibration of the χ values is available. We also note that we used the convention that Hα EW > 0 means that Hα is in emission and Hα EW < 0 means that it is in absorption.

To calculate the $L_{\rm H\alpha}/L_{\rm bol}$ uncertainty, we generated a normal distribution of Hα EW with its literature-reported error as the standard deviation for each star and calculated the $L_{\rm H\alpha}/L_{\rm bol}$ for each value in the normal distribution. We adopted the standard deviation of the final distribution as the error for $L_{\rm H\alpha}/L_{\rm bol}$. We did not include errors of the χ values in the error calculation.

4.2. Unresolved Binary Identification

We performed a search for known external factors that could increase the magnetic activity of the star, such as close binarity (Morgan et al. 2012; Skinner et al. 2017) and accretion disks outside the White & Basri (2003) criteria (see Section 2.3) between our age calibrators. We used the empirical sequences based on bona fide members for each young association (Gagné et al. 2020) to search for photometric binaries by identifying M dwarfs in the binary sequence, hence at most 0.75 brighter in absolute magnitude ($M_{\rm G}$) for a given color ($G - G_{\rm RP}$) than the value indicated by the model. We visually inspected each potential binary in the color–magnitude diagram of its respective young associations, and only selected stars for which we were able to confirm that they lived in the binary sequence. We only applied this method for stars with $G - G_{\rm RP} < 1.2$ because the binary sequence is highly scattered for redder stars. We identified five potential binaries, which are indicated in the age calibrators sample in the column `potential_binary` with a 1. These stars were removed from the following analysis.

For M dwarfs that are comoving with a white dwarf in our sample, we performed a literature search looking for known binaries or other factors that could increase the magnetic activity. All the following cases were removed from the following analysis: 2MASS J18393839+1623136 was identified as an unresolved X-ray binary (Haakonsen & Rutledge 2009), and 2MASS J13545778+0512391 is surrounded by an accretion disk (Theissen & West 2014).

5. Activity Fraction

We used the young part of the sample of age calibrators, described in the previous section, to calculate the activity fraction as a function of color for M dwarfs younger than 1 Gyr and compared it with previous activity studies of field dwarfs. In this section we describe how we classified M dwarfs as active or inactive, and the resulting activity fraction.

5.1. Fitting the Inactive Sequence

Previous studies have identified what we define as the inactive sequence in this study, in Hα EW versus mass or effective temperature for M dwarfs (e.g., Stauffer & Hartmann 1986; López-Santiago et al. 2010; Newton et al. 2017; Fang et al. 2018). This inactive sequence is defined as the lower boundary of the Hα EW versus mass, color, or spectral type relation, and it shows an increase in Hα EW from higher to

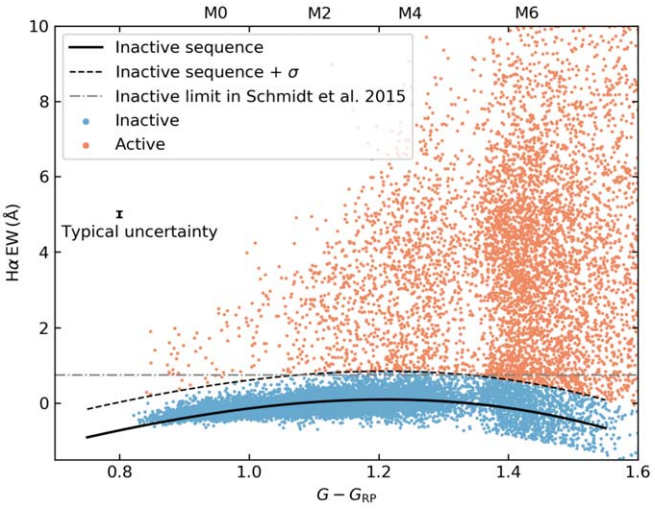

Figure 3. Classification into active and inactive M dwarfs. We fit the inactive sequence shown as a solid black line using the Kiman et al. (2019) sample and defined the boundary between active and inactive stars as the inactive sequence plus δ, where $\delta = 0.75$ Å, shown as the dashed black line. Typical error bars are indicated for the active and inactive stars to the left of the plot. As a comparison, we include the boundary used by Schmidt et al. (2015) as a dash–dotted gray line. We show active stars in orange and inactive stars in blue, classified with our criteria.

lower masses (or redder colors). This increase in Hα EW is related to a decrease in the Hα absorption from the photosphere, meaning a decrease in photospheric luminosity (Stauffer & Hartmann 1986), and not to an increase in emission. We used Kiman et al. (2019) objects to establish the inactive sequence for Hα EW versus $(G - G_{RP})$, and with it, the active or inactive category. To establish the inactive sequence following Newton et al. (2017), we iterated a third-degree polynomial fit to stars with Hα EW < 1 Å 10 times. In each iteration we rejected the stars that had an Hα EW higher than the best fit. We defined the activity boundary as the best fit to the inactive sequence plus a small increment, δ,

$$\begin{aligned} \text{H}\alpha\ \text{EW} = &-2.39 \times (G - G_{RP})^3 \\ &+ 2.84 \times (G - G_{RP})^2 \\ &+ 3.63 \times (G - G_{RP}) - 4.22 + \delta, \end{aligned} \quad (1)$$

where $\delta = 0.75$ Å, and it was added to make our classification into active and inactive compatible with previous definitions (West et al. 2011; Schmidt et al. 2015). This limit is valid in the range $0.8 < (G - G_{RP}) < 1.55$ (M0 $\leqslant$ SpT $\leqslant$ M7). We considered all the stars that have an Hα EW above the boundary to be active. All other objects were considered inactive. We show the activity boundary, the best fit to the inactive sequence, and our classification as active and inactive in Figure 3. As a comparison, we show the limit for active and inactive used by Schmidt et al. (2015). Among other cuts related to the signal-to-noise ratio, Schmidt et al. (2015) considered inactive stars as those with Hα EW < 0.75 Å. Their limit agrees with our definition, except for a small deviation for spectral types <M0 and >M6.

5.2. Calculating Active Fraction as a Function of Age

Using the definition of active and inactive described above, we calculated the active fraction in bins of the red Gaia DR2 color $(G - G_{RP})$ and studied its dependence on age. We used the histogram function available in the Python package `numpy` (Oliphant 2006; Van Der Walt et al. 2011) to define the bins in color because it is optimized for non-normal data. We repeated this calculation for the following age bins: (0–20), (20–60), (100–150), (500–700), and (700–1000) Myr. The results are shown in Figure 4, where we included a reference to the mean spectral type (SpT) for each color at the top of the figure. We also included the activity fraction for the sample from Kiman et al. (2019) in black, which is assumed to be primarily field stars, and it reproduces the results from previous studies (West et al. 2004, 2011; Schmidt et al. 2015). The errors for each point were calculated based on a binomial distribution as

$$\sigma_f = (f \times (1 - f))/n,$$

where f and σ_f are the active fraction and uncertainty, and n is the number of stars in the bin.

By analyzing the active fraction as a function of age in Figure 4, we show that the active fraction of M dwarfs evolves with age. There is a clear difference in the evolution of the active fraction between early- (<M2) and mid-M dwarfs (M4 – M7). While the active fraction for early-M dwarfs decreases from 1 to almost 0 between 0 and 750 Myr, for mid-M dwarfs, the active fraction stays close to 1. This difference between early- and mid-M dwarfs agrees with previous studies, which showed that later-type M dwarfs stay active longer than earlier-type stars (West et al. 2004, 2011; Schmidt et al. 2015).

The active fraction for early-type M dwarfs in Figure 4 decreases progressively from 0 Myr to field-age dwarfs, while for mid spectral types (M4 $\leqslant$ SpT $<$ M7), it seems to decrease more abruptly from (700–1000) Myr (blue line) to field stars (black line). Note that the field active fraction represents a distribution of different ages. Therefore the difference between the bins (700–1000) Myr and field for mid-type M dwarfs could be indicating that late types stay active longer, and we do not have a high enough age resolution to distinguish the progressive decrease of the active fraction with age. This discrepancy might also indicate that the magnetic activity of mid-type M dwarfs decreases more abruptly than for early-types.

Both (500–700) and (700–1000) Myr age bins (the two blue lines) are statistically equivalent and present a transition period centered at M2, where the active fraction increases from 0 to 1, for $1.0 < (G - G_{RP}) < 1.2$. Significantly, this transition is completed close to spectral type ~M3, the limit between partially and fully convective M dwarfs (Chabrier & Baraffe 1997). The shape of this transition for both bins could be affected by other physical effects that increase the magnetic activity of a star. For example, the active fraction could increase because of close companions of the stars, which increase their magnetic activity (e.g., Kraus et al. 2011; Morgan et al. 2012; Dhital et al. 2015; Skinner et al. 2017). For the colors $1.0 < (G - G_{RP}) < 1.1$, the fraction of active stars is 20%, which is close to the multiplicity fraction of M dwarfs of (23.9 ± 1.4)% at separations <50 au found by Winters et al. (2019). We searched the literature for references of binarity and we did not find known binaries for these stars. Also, our sample is not complete, so we cannot compare directly to the results in Winters et al. (2019). Follow up observations are necessary to distinguish if these stars are still active at ~700 Myr, or they have an unresolved binary keeping them active.

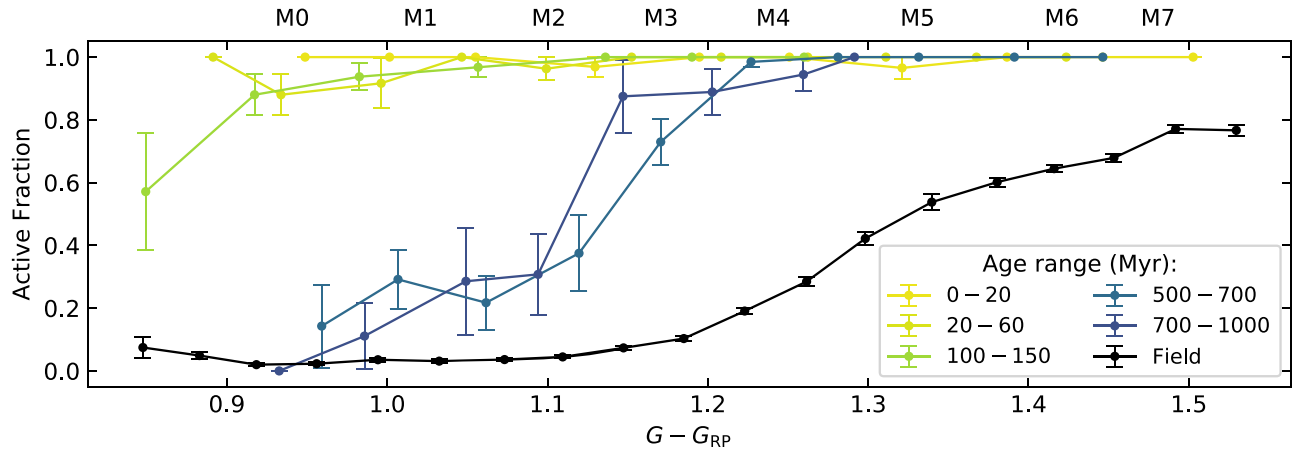

Figure 4. Active fraction per bins of the Gaia red color for different bins of age. We include the active fraction for field M dwarfs calculated from the sample of Kiman et al. (2019) in black. We note that the active fraction decreases with age for M dwarfs and that this decrease depends on mass.

6. Updated Age–Activity Relation for Active M Dwarfs

6.1. Characterizing Hα versus Age

We used our calibrators for Hα EW and $L_{H\alpha}/L_{bol}$ to study the activity strength as a function of age (Figures 5(a) and (b), respectively). We divided the calibrators into three panels according to their spectral type: M0 – M2, M3 – M6, and M7 – M9, which roughly correspond to early-type partially convective, mid-type fully convective, and ultracool fully convective M dwarfs, respectively. In the $L_{H\alpha}/L_{bol}$ plots we only show active stars. Inactive stars have $L_{H\alpha}/L_{bol}$ with a too low signal-to-noise ratio to be significant (the gray area in Figure 5(a)).

There is a large spread of Hα EW between early-, mid-, and late-type M dwarfs, especially at the younger ages, shown in Figure 5(a). As indicated by previous studies (e.g., Stauffer & Hartmann 1986; West et al. 2011; Schmidt et al. 2015), Hα EW increases from early- to late-M dwarfs of the same age, which explains this effect, and it is removed when $L_{H\alpha}/L_{bol}$ is calculated, as can be seen in Figure 5(b).

We found fewer than 10 mid- and late-type old (>1 Gyr) active M dwarfs according to their Hα EW, and no early types. We could not identify any external factors related to these stars, such as a close binary, which would increase their magnetic activity. Therefore we consider them to be true active stars (see Section 4.2). The three youngest late-type M dwarfs in the $L_{H\alpha}/L_{bol}$ are not displayed in the Hα EW plot because their EW values are higher than 25 Å and thus are outside of the axis limit.

We also note that there are stars in the inactive region at all ages in Figure 5(a) (Hα EW $\lesssim$ 0.75 Å, gray area), meaning that a small Hα EW does not necessarily indicate old age for an M dwarf. However, we do see an increase in the number of stars with low Hα EW in the inactive region as age increases.

To study the trends of activity strength with age, we calculated the median values, 25 and 75 percentile for a sliding window of width 0.8 in units of $\log_{10}$(Age/yr) for both Hα EW and $L_{H\alpha}/L_{bol}$. The results are shown in Figures 6(a) and (b), respectively. The relation between Hα EW and age for early-M dwarfs (purple lines in Figure 6(a)) shows a gradual decline from approximately 5 to 0 Å in ∼1 Gyr. For mid spectral types (M3 – M6, orange lines) we observe a progressive decrease of Hα EW with age until ∼1 Gyr. After 1 Gyr, we observe a large decline in Hα (ΔHα EW ∼ 4 Å). There are too few late-type dwarfs in our sample for us to be able to make a robust conclusion. However, we do observe a decline in the value of Hα EW with age.

$L_{H\alpha}/L_{bol}$ presents a similar decay of magnetic activity for early and mid types (purple and orange lines) for ages <1 Gyr in Figure 6(b). After this age, early-type M dwarfs are all inactive in our sample, while mid-type M dwarfs present a transition to a steeper decrease of the magnetic activity with age. However, we need more old M dwarfs with Hα measurements to conclude about the evolution of magnetic activity after 1 Gyr.

There is significant scatter both in Hα EW and $L_{H\alpha}/L_{bol}$ at each age bin, partially due to the intrinsic variability of Hα (Lee et al. 2010; Bell et al. 2012). To study the scatter in more detail, we analyzed the M dwarfs in our sample that have duplicate measurements of Hα EW. Some of these duplicated stars come from different studies of the same young association, which performed their own Hα EW measurements. We also noticed that the duplicated age calibrators are, on average, at a slightly shorter distance than non-duplicated age calibrators. This tendency may be due to these stars being more likely to be selected by studies given the better quality of the data. We see no such tendency with spectral type. Therefore we are confident that we can use these duplicated measurements to study Hα variability. Our sample of age calibrators contains 155 stars with 2–6 independent measurements of Hα EW, which are shown in the top panel of Figure 7, with the different measurements of Hα EW corresponding to the same star joined by a line. We also show the difference between the maximum and minimum value of Hα EW for each star in the bottom panel of Figure 7. We note that 94% of the M dwarfs in the sample have an intrinsic Hα variability $\leqslant$5 Å. By searching the literature for the stars with higher ΔHα EW, we found that most of the stars that have ΔHα EW $\geqslant$ 10 Å are known as variable stars (Kiraga 2012; Schmidt et al. 2015; Samus et al. 2017). This analysis of the variability shows that our 3 Å cut to distinguish compatible measurements was conservative (see Section 2.2). We also note that there is a correlation between

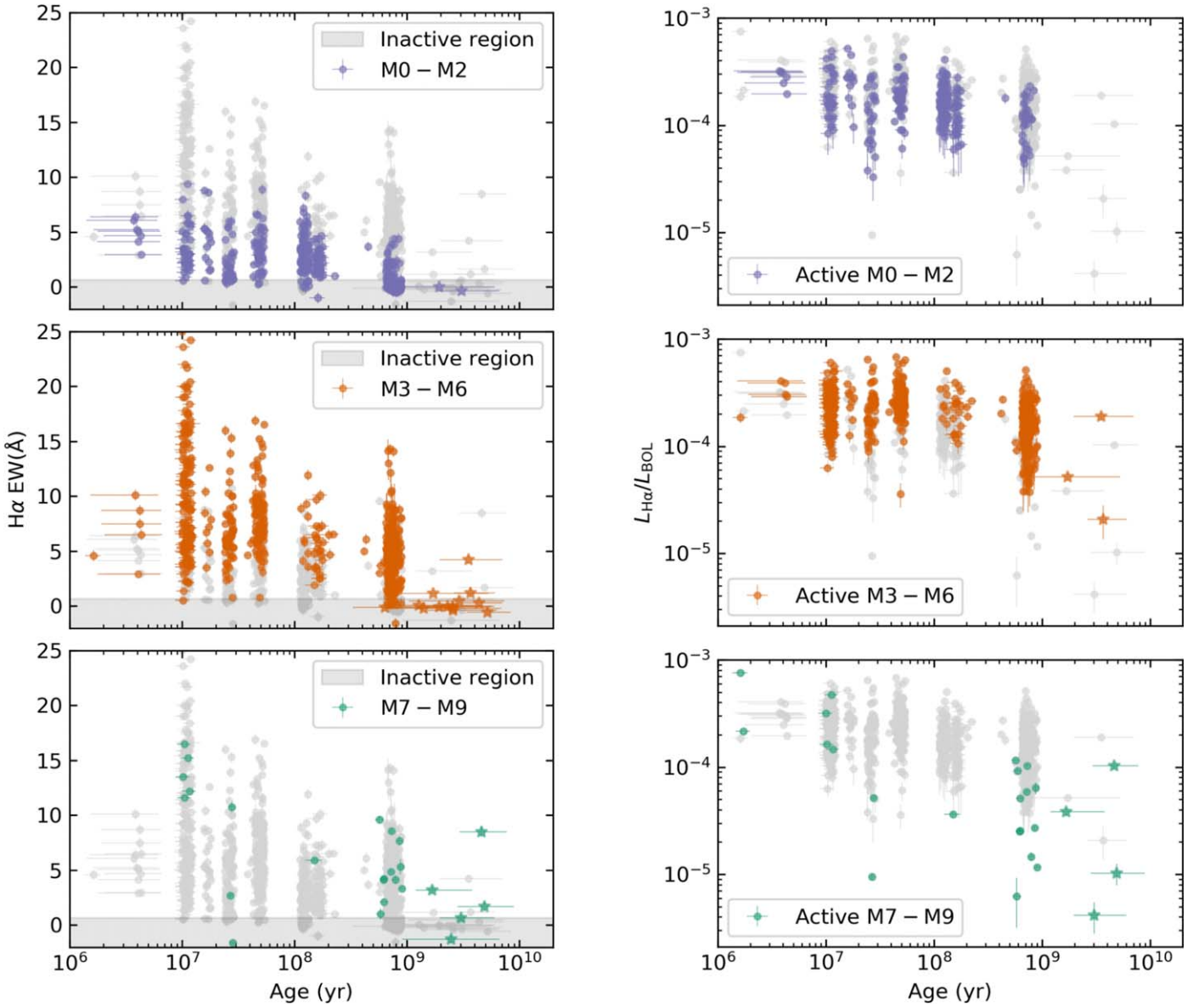

(a) Hα EW (b) $L_{H\alpha}/L_{bol}$

Figure 5. Age activity relation as indicated by the Hα equivalent width (Hα EW in the left panels) and fractional Hα luminosity ($L_{H\alpha}/L_{bol}$ in the right panels). We divided the sample into three panels according to the spectral type: in purple we show early partially convective M dwarfs (M0 − M2, top panels), in orange we plot mid fully convective M dwarfs (M3 − M6, middle panels), and in green we show ultracool fully convective M dwarfs (M7 − M9, bottom panels). M dwarfs from young associations are shown with a circle, and stars that have a white dwarf companion are shown with a pentagram. A small random shift has been applied to the age of the stars from young associations to improve the visualization. No shift has been applied to the age of the M dwarfs with a white dwarf companion. We added a gray area to approximately indicate the stars that are considered inactive. For the precise definition of inactive, see Figure 3. We only show active stars for the $L_{H\alpha}/L_{bol}$ relation.

ΔHα EW and Hα EW measurements that agrees with the results from Lee et al. (2010) and Bell et al. (2012).

6.2. Fitting the Age–Activity Relation

We fit the age–activity relation measured with $L_{H\alpha}/L_{bol}$ for all active age calibrators (856 stars, Tables 2 and 1) without binning by spectral type ranges, given that we lack enough information per bin. A broken power law has been used in several previous studies of the X-ray age–activity relation (e.g., Jackson et al. 2012; Booth et al. 2017) and for the rotation-activity relation (e.g., Delfosse et al. 1998; Douglas et al. 2014; Núñez et al. 2016; Newton et al. 2017) for cool dwarfs to model a saturation regime where $L_{H\alpha}/L_{bol}$ remains constant, followed by a power-law decay. Furthermore, West et al. (2008a) found that for M dwarfs, $L_{H\alpha}/L_{bol}$ remains constant for young ages and then decays. Therefore we decided to use a broken power law to fit the age–activity relation. See Appendix B for a comparison of the broken power law and polynomials of different degrees using the cross-validation method.

We performed an MCMC fit to the age–activity relation using `emcee` (Foreman-Mackey et al. 2013) to estimate the

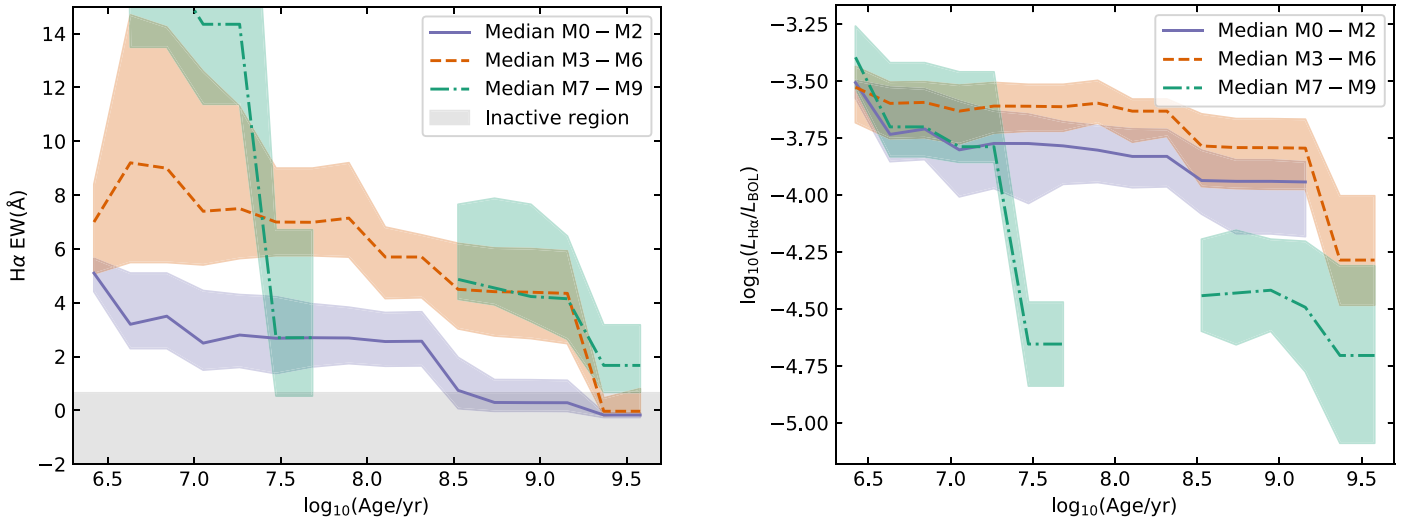

(a) Hα EW (b) $L_{\mathrm{H}\alpha}/L_{\mathrm{bol}}$

Figure 6. Median values and 25 and 75 percentile for a sliding window of width 0.8 in units of $\log_{10}$(Age/yr) for both Hα EW and fractional Hα luminosity ($L_{\mathrm{H}\alpha}/L_{\mathrm{bol}}$). Figure 5 shows the data used to make this figure. We note that the magnetic activity for early-type M dwarfs decreases progressively, while for mid-type M dwarfs, it seems to decrease rapidly after 1 Gyr.

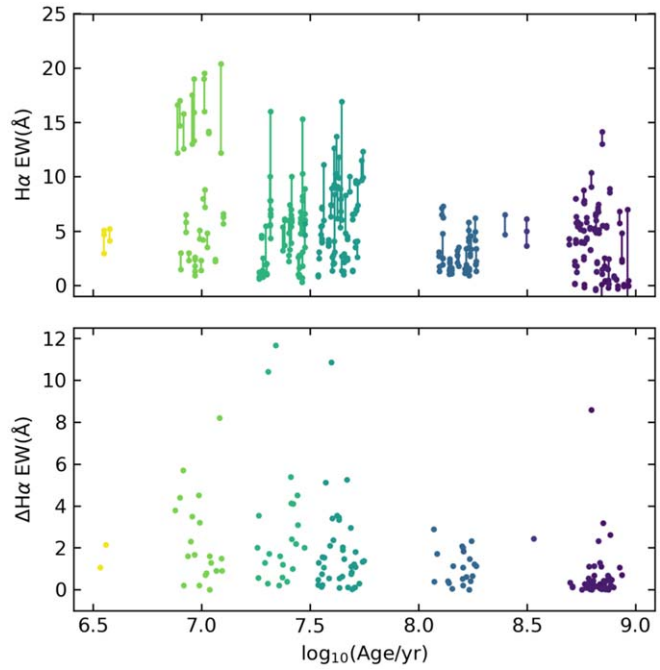

Figure 7. Hα variability from repeated independent measurements of the same stars as a function of age. A small random shift has been applied to the age of each star to improve visualization, so we also color-coded the stars according to their age to keep track of it. In the top panel we show all the measurements for each star. Measurements of the same star are connected with a line. In the bottom panel we show the difference between the maximum and minimum values of Hα EW for each star. We found that 94% of the repeated stars have a level of Hα EW variability $\leqslant$5 Å at young ages (<1 Gyr).

parameters of the broken power law and their uncertainties. The broken power law we fit to the relation was of the form

$$\log_{10}\left(\frac{L_{\mathrm{H}\alpha}}{L_{\mathrm{bol}}}\right)_{\mathrm{model}} = \begin{cases} \alpha_1 \log_{10}\dfrac{t}{t_0} + \beta_1, & t < t_0 \\ \alpha_2 \log_{10}\dfrac{t}{t_0} + \beta_1, & t_0 \leqslant t, \end{cases} \tag{2}$$

where t is the age of the star. We used a Gaussian function as the likelihood and uniform priors on each parameter. As discussed before, the age–activity relation for Hα is scattered due in part to the intrinsic variability of this emission line. We included an additional parameter, σ_v, to model the intrinsic variability of Hα assuming that the variability of $\log_{10}(L_{\mathrm{H}\alpha}/L_{\mathrm{bol}})$ is the same for all stars, in other words, that the Hα intrinsic variability is proportional to Hα EW (Lee et al. 2010; Bell et al. 2012). The resulting likelihood for our model is

$$\begin{aligned} \log \mathcal{L} = &-\frac{1}{2} \\ &\times \sum_i \frac{\log_{10}\left(\frac{L_{\mathrm{H}\alpha}}{L_{\mathrm{bol}}}\right)_i - \log_{10}\left(\frac{L_{\mathrm{H}\alpha}}{L_{\mathrm{bol}}}\right)_{\mathrm{model}}(t_i)}{\sigma^2_{\log_{10}\left(\frac{L_{\mathrm{H}\alpha}}{L_{\mathrm{bol}}}\right),i} + \sigma_v^2} \\ &+ \log\left(\sigma^2_{\log_{10}\left(\frac{L_{\mathrm{H}\alpha}}{L_{\mathrm{bol}}}\right),i} + \sigma_v^2\right), \end{aligned} \tag{3}$$

where we sum over each measurement i of $L_{\mathrm{H}\alpha}/L_{\mathrm{bol}}$ and age.

To ensure that the MCMC had converged, we calculated the autocorrelation time (τ_f) for our likelihood and sampled our posterior by performing 100 τ_f steps to ensure ~100 independent samples.[17]

We show the maximum likelihood of the parameters of the broken power law and the σ_v over the age calibrators in Figure 8, as well as 100 random samples from the posterior distributions of the broken power-law parameters. We show the full posterior distributions and the maximum likelihood values for each parameter in Figure 9. As discussed in Section 6.1, we found for $\log_{10}(L_{\mathrm{H}\alpha}/L_{\mathrm{bol}})$ a decrease in activity strength from 1 Myr to $t_0 \sim 776$ Myr with a power-law index of $\alpha_1 = -0.11^{+0.02}_{-0.01}$, with a variability of $\sigma_v = 0.22 \pm 0.01$. For ages >776 Myr, the relation shows a decline in magnetic activity with a power-law index of $\alpha_2 = -0.88^{+0.20}_{-0.25}$. However,

[17] To calculate the autocorrelation time, we followed the tutorial in https://emcee.readthedocs.io/en/stable/tutorials/autocorr/.

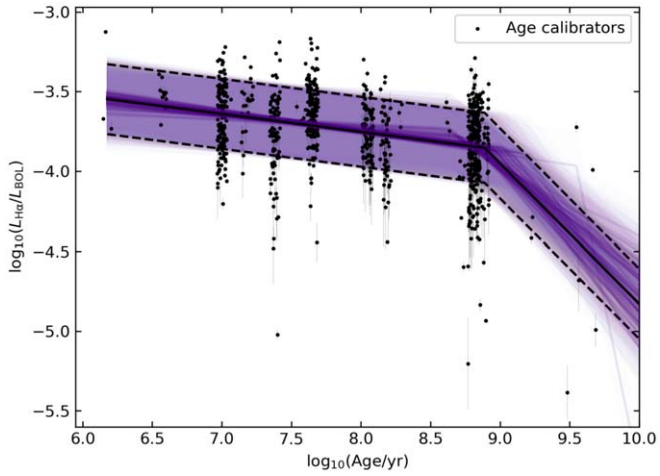

Figure 8. Age activity relation for $L_{H\alpha}/L_{bol}$ for M dwarfs. We fit the relation with a broken power law using an MCMC. We show as a black line the maximum likelihood fit and as a dashed black line the fit $\pm \sigma_v$, which models the Hα variability. We also include 100 draws from the posterior distributions for the parameters of the fit in purple. The age calibrators are shown as black points, and we added a random shift to their ages to facilitate visualization. Our model fits most of the younger stars (<1 Gyr) well, and the range of variability includes the denser areas of points. However, we do not have enough information to fit the breaking point or the power-law decay of the older stars.

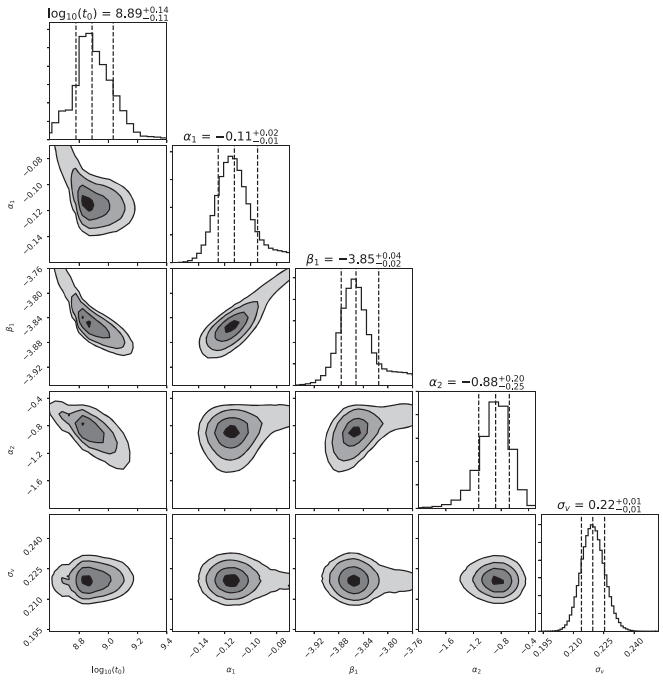

Figure 9. Posterior probabilities for each parameter of the broken power law we fit to the age–activity relation in Figure 8.

t_0 and the power-law index for old stars are based on fewer than 10 active old stars. Therefore these parameters are not well constrained with our data, as is shown by the purple line fits in Figure 8. We do not recommend using this fit for stars with ages >776 Myr. More data for older ages are needed to calibrate the decay. From Figure 8 we can conclude that there is a breaking point at which the magnetic activity starts to decline with a steeper slope according to Hα, and that it is at an age >776 Myr, as indicated by our t_0 parameter. As shown in Figure 5(b), the old active stars are of spectral type $\geqslant$M3, therefore this breaking point corresponds to late-type stars alone. We note that this age activity relation was obtained using only active stars. We will develop a model combining $L_{H\alpha}/L_{bol}$, the active fraction, color, and age in future work.

7. Comparison to Previous Age–Activity Relations

West et al. (2006) studied the Hα age–activity relation by collecting a sample of M dwarfs with 3D positions, 3D kinematics, and Hα EWs and luminosities. They found that $L_{H\alpha}/L_{bol}$ decreases with increasing vertical distance from the galactic plane and that the slope of the relation depends on the spectral type. As vertical distance is an age indicator such that older stars are located farther from the plane (Wielen 1977; Hänninen & Flynn 2002), their conclusion was that $L_{H\alpha}/L_{bol}$ decreases with increasing age. They also found that the active fraction of M dwarfs also decreases with vertical height. West et al. (2008b) used a one-dimensional model to simulate the dynamics of stars in the Galaxy and fit the relation between active fraction and vertical height. They found that the active lifetime of M dwarfs increases from 0.8 to 8 Gyr with spectral type (M0 to M7), meaning that later-type M dwarfs stay active longer than early-type ones. The results from our study of the active fraction as a function of color for different ages (Figure 4) agrees with the results from West et al. (2006) and other works that reported a similar analysis (e.g., Hawley et al. 1996; West et al. 2011; Schmidt et al. 2015). In addition, our age–activity relation (Figures 5, 6, and 8) qualitatively agrees with the results from West et al. (2008b).

West et al. (2008a) used a similar simulation as the we described above to find ages from the vertical height of the stars, and studied the relation between $L_{H\alpha}/L_{bol}$ and age for M2-M7 dwarfs. These relations are plotted as dot–dashed lines in Figure 10 for M2, M5, and M7 over the data for our age calibrators, which are divided according to spectral type range. We also included our results for the fit from Figure 8 as reference. We do not have enough M dwarf-white dwarf pairs with Hα EW measurements to constrain the power-law index for ages >1 Gyr, so we did not include this part of the fit. We found that West et al. (2008a) overestimated the value of the activity strength for early-type M dwarfs and slightly underestimated it for late-type M dwarfs. Their relation also indicates that $L_{H\alpha}/L_{bol}$ remains constant for young ages up to the decline for all M dwarfs. Our fit describes the data better, and unlike West et al. (2008a), we found that $L_{H\alpha}/L_{bol}$ for early- and mid-type M dwarfs decreases progressively for ages <1 Gyr with a slope $\alpha_1 = -0.11^{+0.02}_{-0.01}$. As shown by the relation of the Hα EW and age for each spectral type bin in Figure 6(a), the magnetic activity of old (>1 Gyr), mid-, and late-type M dwarfs seems to decline more rapidly than that of young stars, in agreement with West et al. (2008a). However, we found that early-type M dwarfs become progressively inactive, unlike their result, which indicates a steep decline.

The age–activity relation has been studied for other magnetic activity indicators. Stelzer et al. (2013) used a 90% complete sample of M dwarfs within 10 pc and found that the fluxes of Hα, X-ray, and UV are correlated. This correlation was expected given that the three parameters are indicators of magnetic activity. Therefore we also compared our results to X-ray and UV age–activity relations. Jackson et al. (2012) studied the age–activity relation using the X-ray luminosity for young F, G, and K dwarfs from known young associations (<1 Gyr) and found a saturated region for ages <100 Myr where the X-ray luminosity remains constant and then declines

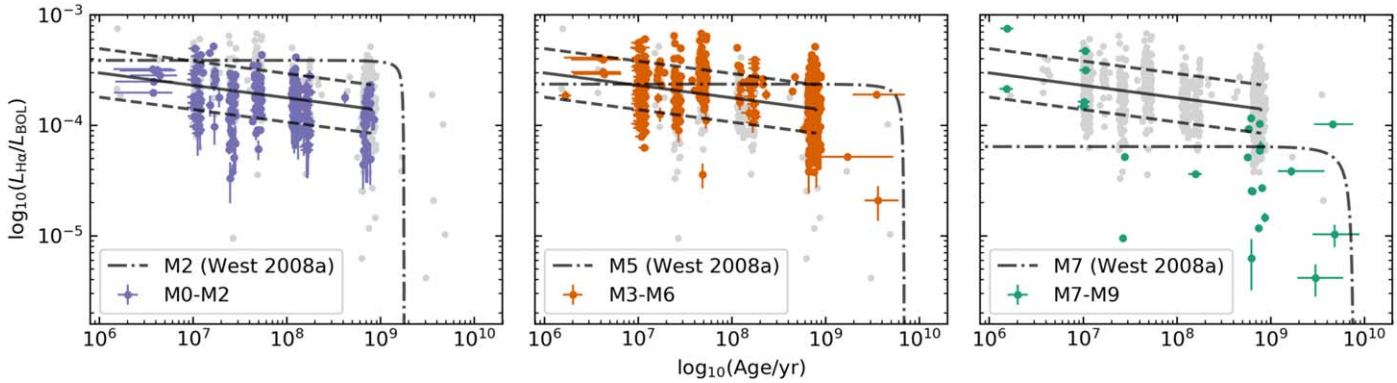

Figure 10. Comparison of our result for the age–activity relation for $L_{H\alpha}/L_{bol}$ with the results from West et al. (2008a). We divided our age calibrators into three spectral type bins: in purple we show early partially convective M dwarfs (M0 − M2), in orange we plot fully convective mid-M dwarfs (M3 − M6), and in green we show ultracool fully convective M dwarfs (M7 − M9). We show as a dot–dashed line the age–activity relation obtained by West et al. (2008a) for M2, M5, and M7. We also show our results for the fit for ages <1 Gyr as a black line and our fit to the variability as dashed black lines.

with a power-law index between $\alpha = -1.09 \pm 0.28$ and -1.40 ± 0.11. Booth et al. (2017) also studied the dependence of X-ray luminosity for a sample of F, G, K, and M dwarfs with ages obtained from astroseismology or from white dwarf co-movers, such that the stars had an age >1 Gyr. They found that the X-ray luminosity decreases with age with a power-law index of $\alpha = -2.8 \pm 0.72$. Instead of a saturated region where $L_{H\alpha}/L_{bol}$ remains constant, we found that magnetic activity for stars with ages <1 Gyr decreases with a small power-law index of $\alpha_1 = -0.11^{+0.02}_{-0.01}$ and for stars >1 Gyr of $\alpha_2 = -0.88^{+0.20}_{-0.25}$ (Figures 8 and 9). Although α_2 is not well constrained by our model, our results seem to agree with those of Jackson et al. (2012) and Booth et al. (2017) in that the decrease in magnetic activity is faster for old than for young stars (<1 Gyr).

Schneider & Shkolnik (2018) studied a sample of M dwarfs from young associations (<1 Gyr) and compared it to field dwarfs to characterize the UV age–activity relation. They found that mid- to late-M dwarfs (0.08–0.35 $M_\odot$) remain relatively active throughout their lifetimes according to the UV flux density, with only a small decrease in magnetic activity from young to field ages. They also found that early-M dwarfs (0.35–0.6 $M_\odot$) have a much more significant decrease in magnetic activity over the same age range. This result agrees with our result for the evolution of the magnetic activity using Hα. For the active fraction as a function of $(G - G_{RP})$ color for different age bins in Figure 4, we found that the active fraction of early-type M dwarfs decreases from 1 to almost zero for field dwarfs, while the active fraction for mid-type M dwarfs remains close to one for ages <1 Gyr and declines at an older age.

8. Conclusions

In this study, we analyzed the age dependence of the magnetic activity of M dwarfs from three complementary perspectives: (1) the dependence of the active fraction of spectral subtypes on age, (2) the dependence of Hα EW on age, and (3) the dependence of fractional Hα luminosity ($L_{H\alpha}/L_{bol}$) on age. We compiled a sample of 892 compatible single M0 − M9 dwarfs (1121 in total, including repeated measurements and not compatible measurements) to serve as age calibrators, based on 89,270 M dwarfs with Hα EW measurements collected from the literature, focusing on M dwarf members of young associations or those that are comoving with a white dwarf. We cross-matched our sample with Gaia DR2 to obtain proper motions and parallaxes and found that 97% of our sample were in Gaia DR2. From this sample, we identified 871 M dwarf members of known young associations (<1 Gyr) using Gaia DR2 kinematics and parallaxes, and BANYAN Σ (Gagné et al. 2018), as well as 21 M dwarfs that are comoving with a white dwarf from Gentile Fusillo et al. (2019). The age for M dwarf members of young associations was obtained from the estimated age of their association. For M dwarfs that are comoving with a white dwarf, the age was calculated with the Python package `wdwarfdate` (R. Kiman et al. 2021, in preparation), which is available online.[18] We have made the code used in this work available on Zenodo (Kiman 2021) and GitHub.[19]

We present the results of our analysis as follows:

1. Of the 871 identified members of young associations in this study, 7 are new candidate members (Table 5).
2. We studied the variability of Hα at young ages for 155 M dwarfs with 2–6 independent Hα EW measurements. We found that 94% of the sample have a ΔHα EW $\leqslant 5$ Å for ages >1 Gyr, where ΔHα EW is the difference between the maximum and minimum value of Hα EW (see Figure 7).
3. We confirmed that both Hα EW and $L_{H\alpha}/L_{bol}$ decrease with age for spectral types M0 − M9. We lack a large enough sample to determine a precise trend in late -M dwarfs (>M7). Kiman et al. (2019) found a dependence of $L_{H\alpha}/L_{bol}$ on vertical action dispersion, which is also a proxy for age (Wielen 1977; Hänninen & Flynn 2002). Figure 20 of Kiman et al. (2019) shows that $\log_{10}(L_{H\alpha}/L_{bol})$ decreases from −3.5 to −5 for both mid (M5 $\leqslant$ SpT $\leqslant$ M8) and late spectral types (SpT $\geqslant$ M8), which agrees with the dependence of $L_{H\alpha}/L_{bol}$ on age that we found for M dwarfs that are comoving with white dwarfs (see Figure 5(b)). This result indicates that mid-type M dwarfs (∼M3 − M6) have a similar Hα age–activity relation to ultracool dwarfs (>M6).
4. We classified our age calibrators as active or inactive according to their Hα EW. Using this classification, we calculated the active fraction per color bin. We confirmed that the active fraction increases with color, which is a proxy for decreasing mass, from M0 − M7, in agreement

[18] https://wdwarfdate.readthedocs.io/en/latest/
[19] https://github.com/rkiman/M-dwarfs-Age-Activity-Relation

with West et al. (2004) and Schmidt et al. (2015). Moreover, by calculating the active fraction per color per age bin, we found that the active fraction varies with age according to spectral type: the active fraction of early M dwarfs (<M3) decreases gradually from 1 to close to 0 between 0 and 750 Myr, while later types stay active longer, such that their active fraction stays close to unity for ages <1 Gyr (see Figure 4).

5. We found that the active fraction for early-type M dwarfs in the age-bin 700–1000 Myr is close to the field value (≫1 Gyr), while mid-types have an active fraction close to unity in the age-bin 700–1000 Myr and 0.6 for the field. The difference in active fraction between early and mid-types after 1 Gyr could be indicating that late types stay active longer, and we do not have a high enough age resolution to distinguish the progressive decrease of the active fraction with age. This discrepancy also could be indicating that the magnetic activity of mid-type M dwarfs decreases rapidly after 1 Gyr (see Figure 4).
6. By comparing Hα EW and $L_{\mathrm{H}\alpha}/L_{\mathrm{bol}}$ as a function of age, we found that the magnetic activity strength of early- and mid-type M dwarfs (<M7) gradually decreases during the first Gyr of their lives. After ∼1 Gyr, early- and mid-types seem to behave differently. We found only two early -M dwarfs (<M3), which are both inactive and continue the trend of a gradual decrease of magnetic activity. For mid-type M dwarfs we found 14 old stars, 11 of which are inactive and present a large decline in Hα (ΔHα EW ~ 4 Å), which seems to indicate that the magnetic activity of mid-type M dwarfs decreases rapidly after ∼1 Gyr. However, higher numbers of old stars (>1 Gyr) are needed to make a robust conclusion.
7. We found that the power-law index for the relation between $L_{\mathrm{H}\alpha}/L_{\mathrm{bol}}$ and age—using all spectral types to fit the data—is $\alpha_1 = -0.11^{+0.02}_{-0.01}$ for ages $\lesssim$776 Myr. For older ages, we only have $L_{\mathrm{H}\alpha}/L_{\mathrm{bol}}$ measurements for spectral types ⩾M3 (the early types that were found are inactive). We found a power-law index of $\alpha_2 = -0.88^{+0.20}_{-0.25}$ for ages $\gtrsim$776 Myr, but it is poorly constrained because it was fit on a sample of <10 old active stars; hence we do not recommend using this relation for stars with ages of $\gtrsim$776 Myr (see Figures 8 and 9). We conclude that spectral types ⩾M3 show a sharp decrease in Hα at ages $\gtrsim$776 Myr. More Hα EW measurements of M dwarfs that are comoving with white dwarfs are needed to fit the age–activity relation for older ages.

In this study we did not take metallicity into account to calibrate the age–activity relation. Previous studies have shown that the metallicity is a source of scatter for the relation between magnetic activity indicators and age: as the metallicity increases, the convection becomes more efficient, which enhances chromospheric activity (e.g., Lyra & De Mello 2005; Lorenzo-Oliveira et al. 2016). Metallicity should not affect the age relation obtained from young associations given than those used in this study have similar values (Malo et al. 2014b). While metallicity might affect the relation for older stars, we are not setting a strong constraint on the age relation for older stars, so it does not modify our conclusions.

This work represents a great advancement in the understanding of the magnetic activity and evolution of M dwarfs. In addition, this work is key for studying star-planet interactions, identifying habitable exoplanets, and identifying true planet signals with the radial velocity method, which can be affected when the host star is magnetically active (ex. Robertson et al. 2013). In future work, we plan to model the relation between Hα EW and age using the calibration from this study. We will use this model in a Bayesian algorithm to estimate ages of individual M dwarfs from their Hα EW combined with other age indicators to improve the precision and accuracy of M dwarf ages.

The authors would like to thank Evgenya Shkolnik and Amelia Bayo for helpful references of Hα EW measurements and Jeff Andrews, Alejandro Núñez, and Siyi Xu for great discussions. The authors would also like to thank John Bochanski for the helpful comments on the paper.

Support for this project was provided by a PSC-CUNY Award, jointly funded by The Professional Staff Congress and The City University of New York.

This material is based upon work supported by the National Science Foundation under grant No. 1614527.

This work has been supported by NASA K2 Guest Observer program under award 80NSSC19K0106.

This work was supported by the SDSS Faculty and Student Team (FAST) initiative.

Support for this work was provided by the William E Macaulay Honors College of The City University of New York.

Software: TOPCAT (Taylor 2005); `emcee` (Foreman-Mackey et al. 2013); `scipy` (Virtanen et al. 2020); `numpy` (Oliphant 2006; Van Der Walt et al. 2011); `matplotlib` (Hunter 2007); `Astropy` (Astropy Collaboration et al. 2013; Price-Whelan et al. 2018); `wdwarfdate` (R. Kiman et al. 2021, in preparation).

Appendix A
Color–Magnitude Diagrams of Young Association Members Used in This Study

In this section we compare the position in the Gaia color–magnitude diagram of the stars we used as members of young associations in this study, with the position of candidate members of each young association (Gagné et al. 2018), and empirical sequences based on bona fide members of young associations of different ages (Gagné et al. 2020). The color–magnitude diagrams for each young association are shown in Figure 11. We conclude that the stars we used in this study as members are not discarded based on the color–magnitude diagrams: although some stars do not follow the corresponding age sequence, they present a similar scatter as the candidate members (light blue empty circles). More studies of these systems are needed before they are confirmed as members.

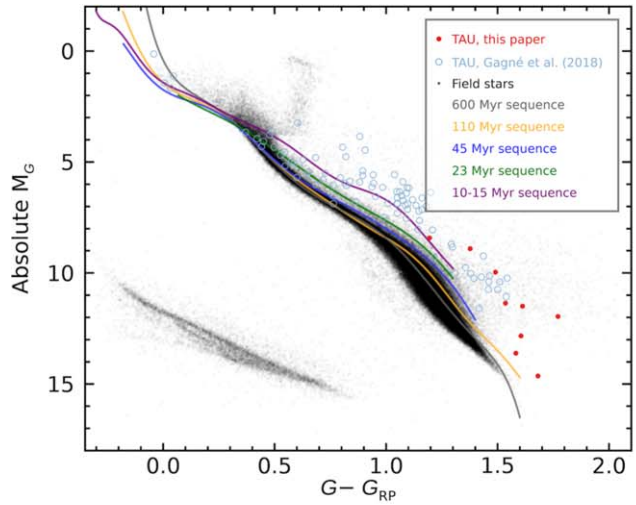

(a) Taurus, 1.5 ± 0.5 Myr.

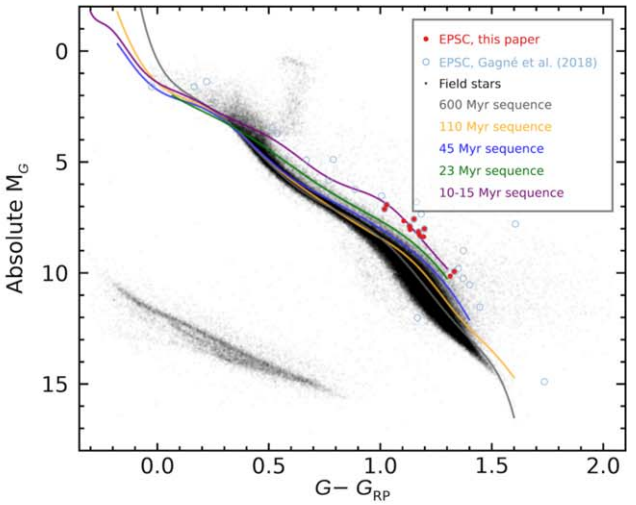

(b) ϵ Chamaeleontis, 3.7 ± 4.6 Myr.

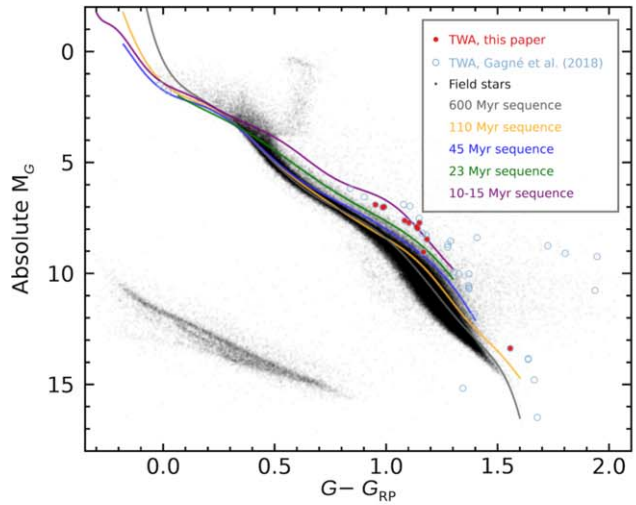

(c) TW Hya, 10.0 ± 3.0 Myr.

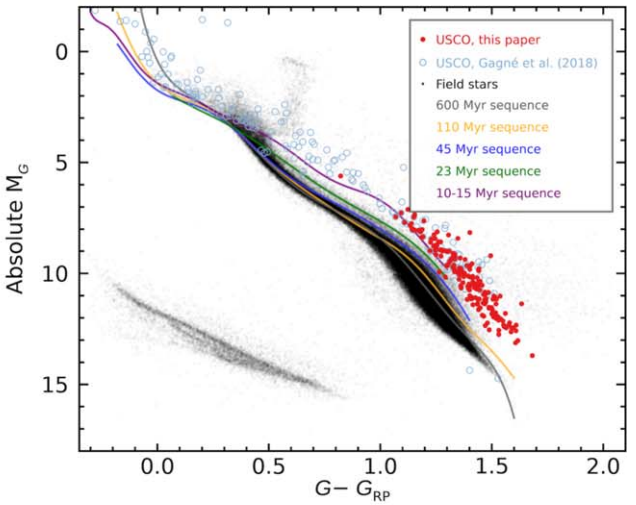

(d) Upper Scorpius, 10.0 ± 3.0 Myr.

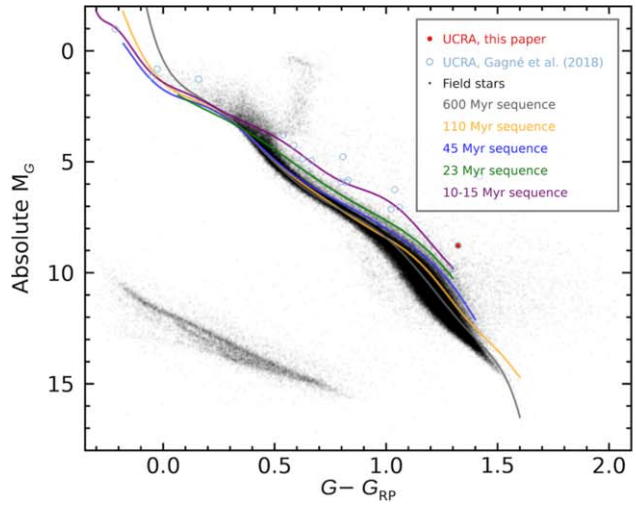

(e) Upper CrA, ~ 10 Myr.

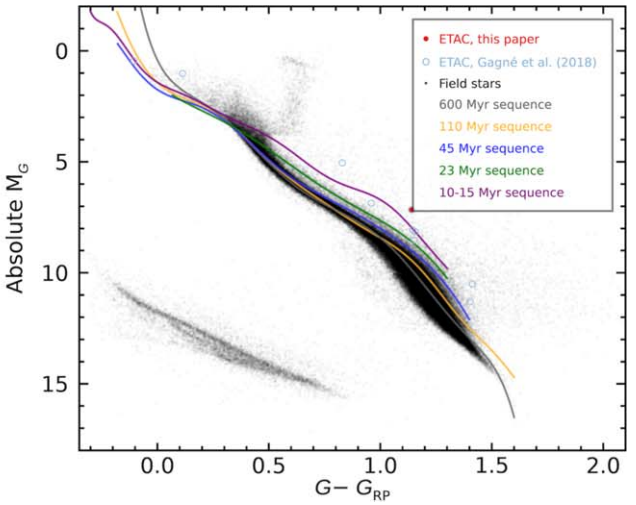

(f) η Chamaeleontis, 11.0 ± 3.0 Myr.

Figure 11. CMDs comparing stars we used as members of young associations in this study (red circles) with candidate members of each association (light blue empty circles; Gagné et al. 2018). We also show a sample of field stars from Gaia DR2 in black, and the empirical sequences based on bona fide members of young associations for the ages of 10–15, 23, 45, 110, and 600 Myr (Gagné et al. 2020). The position in the CMD does not discard any of stars we used in this study as members.

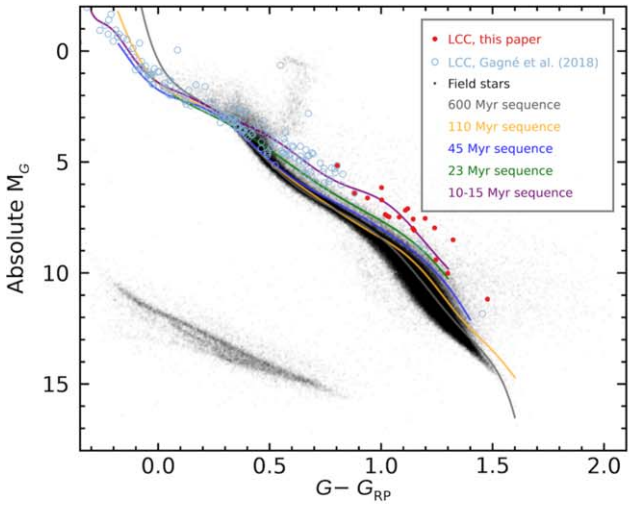

(g) Lower Centaurus Crux, 15.0 ± 3.0 Myr.

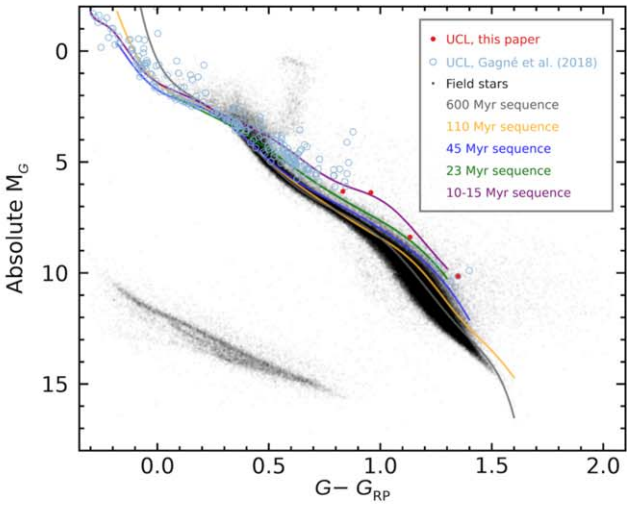

(h) Upper Centaurus Lupus, 16.0 ± 2.0 Myr.

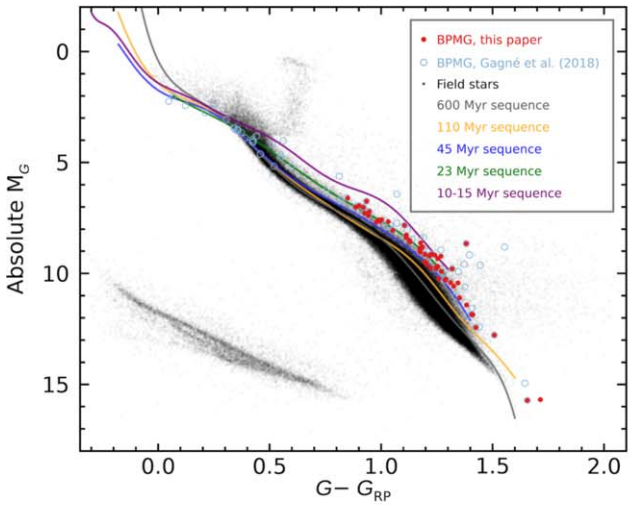

(i) β Pictoris, 24.0 ± 3.0 Myr.

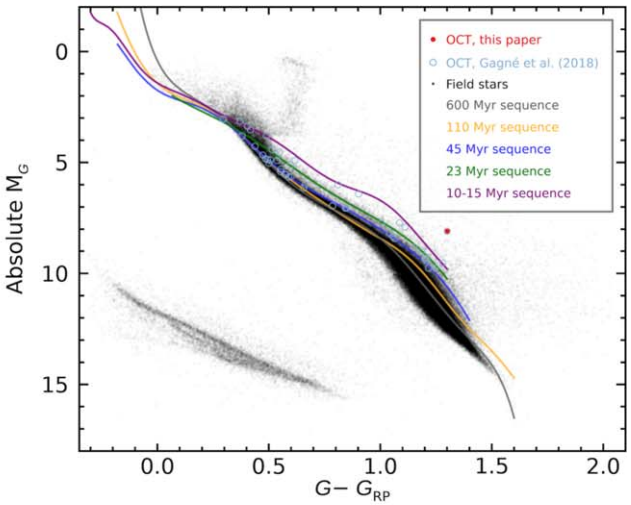

(j) Octans, 35.0 ± 5.0 Myr.

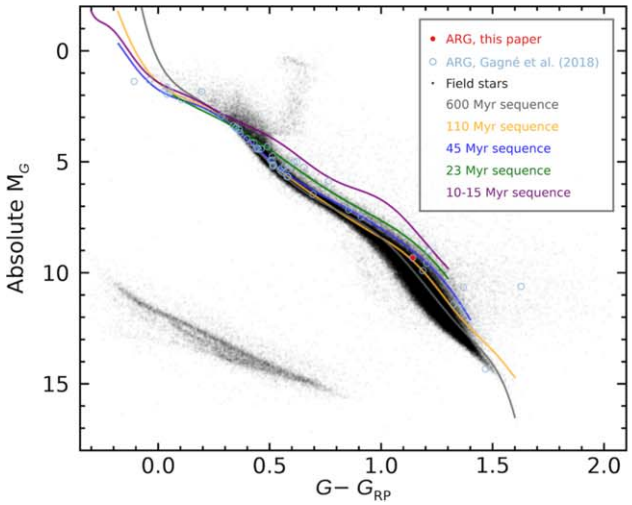

(k) Argus, $40 - 50$ Myr.

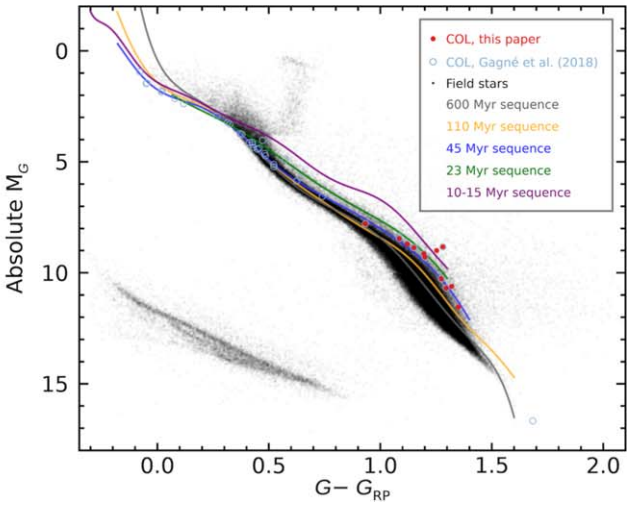

(l) Columba, 42.0 ± 6.0 Myr.

Figure 11. (Continued.)

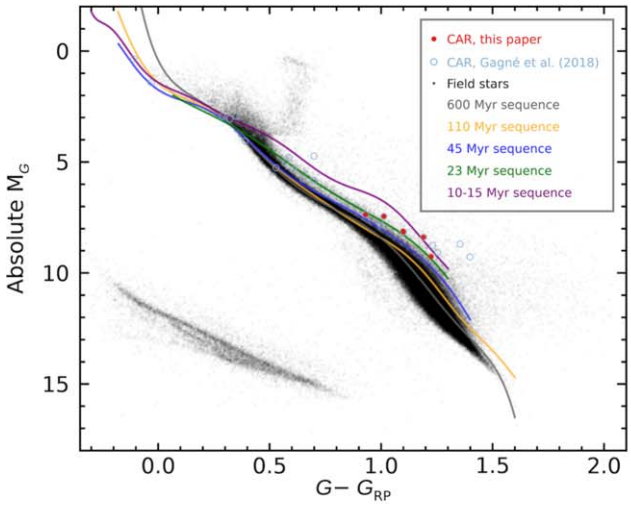

(m) Carina, 45.0 ± 11.0 Myr.

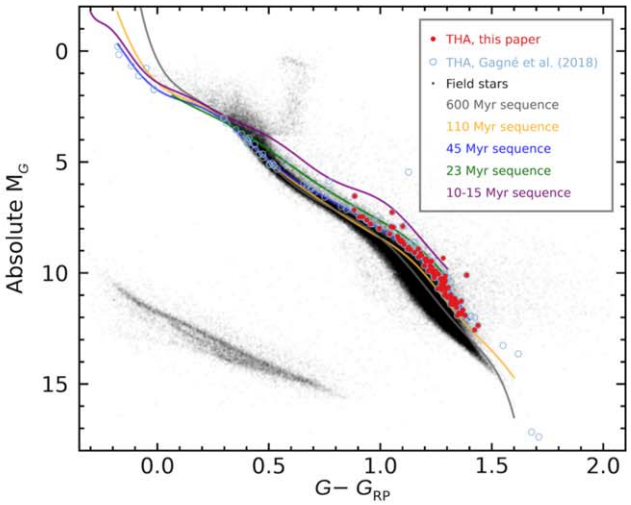

(n) Tucana-Horologium association, 45.0 ± 4.0 Myr.

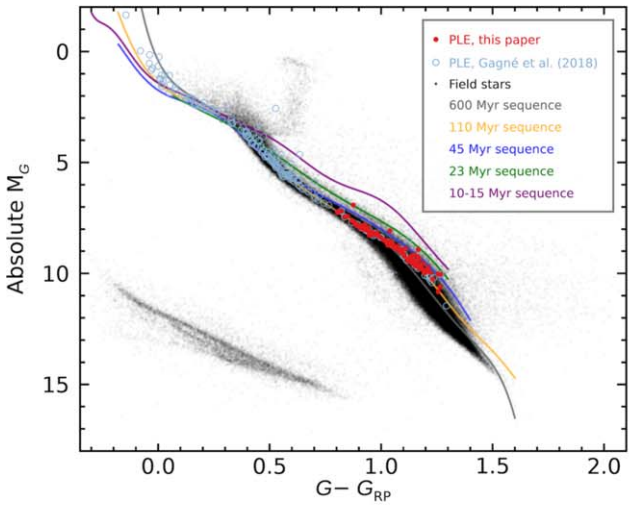

(o) Pleiades cluster, 112 ± 5 Myr.

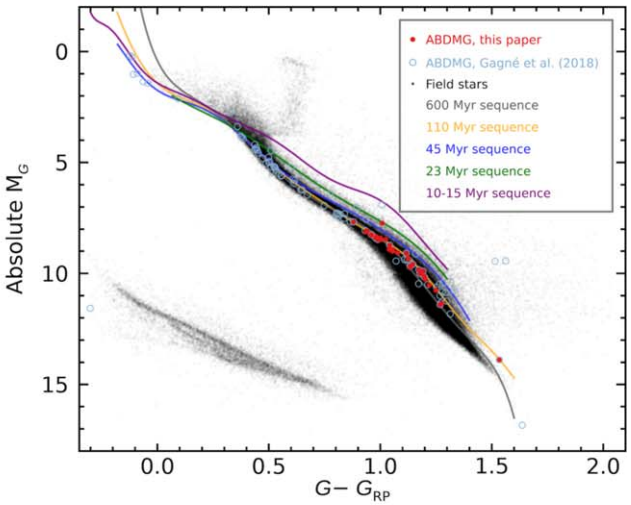

(p) AB Doradus, 149.0 ± 51.0 Myr.

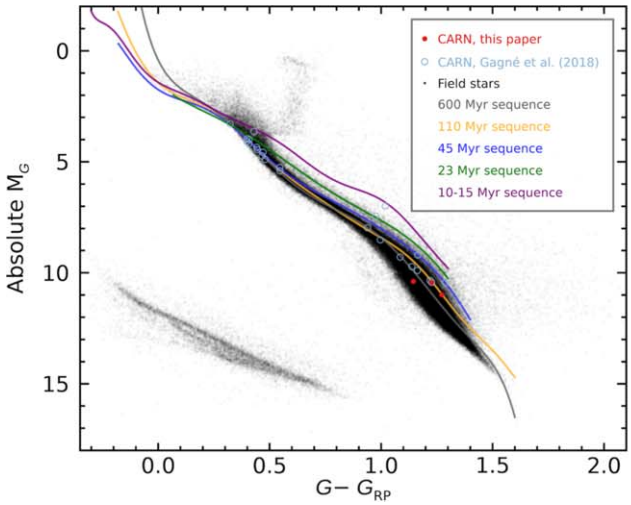

(q) Carina-Near, 200.0 ± 50.0 Myr.

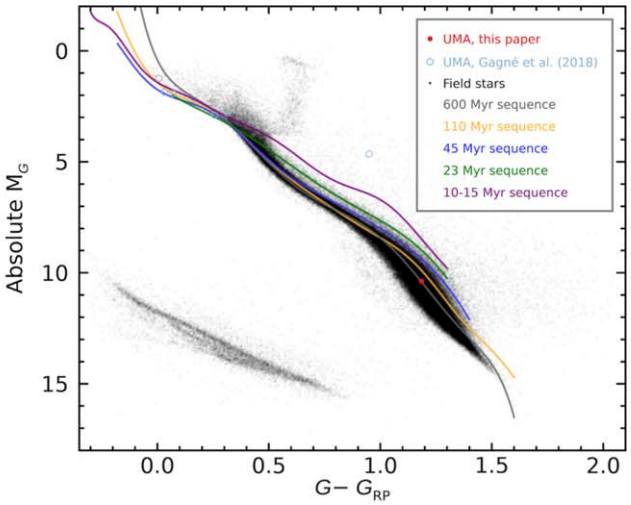

(r) core of the Ursa Major cluster, 414.0 ± 23.0 Myr.

Figure 11. (Continued.)

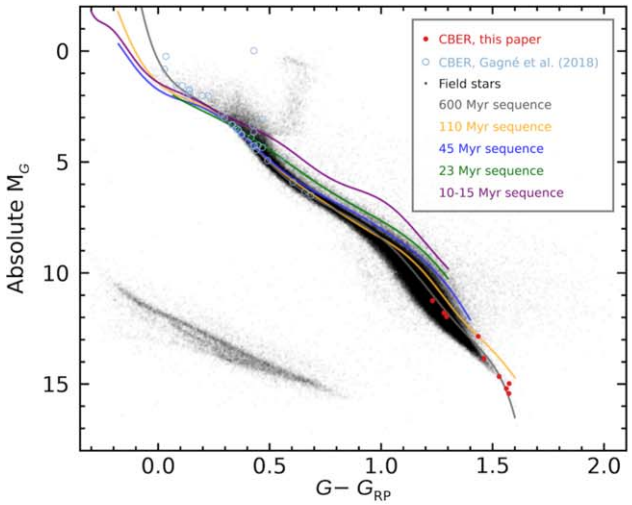

(s) Coma Berenices, 562.0 ± 98.0 Myr.

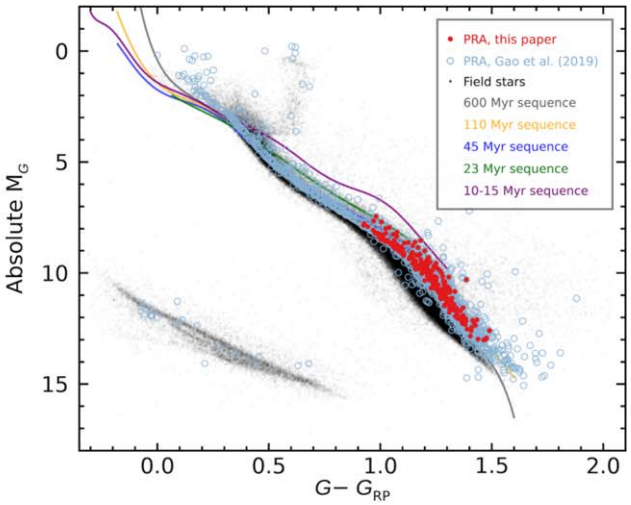

(t) Praesepe cluster, 650.0 ± 50.0 Myr.

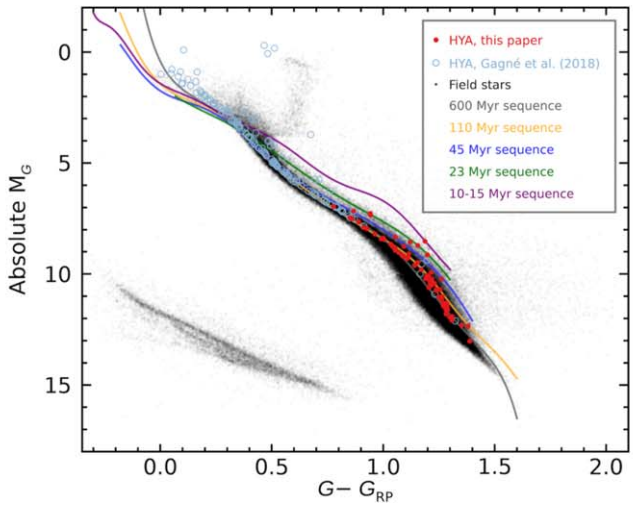

(u) Hyades cluster, 750.0 ± 100.0 Myr.

Figure 11. (Continued.)

Appendix B
Comparison Models for Fitting the Age–Activity Relation

Previous studies have used the broken power law to fit age–activity relations (see Section 6.2). As we are interested in the predictive power of our model, we tested the broken power law against polynomials of degrees 1 to 6 using a cross-validation method. In this method, we leave one of the calibration stars out and fit the rest with one of the models we wish to compare. Then we use the fitted model to predict the value of the left-out element, and we calculate how close the predicted value is to the true value. The total score for each model is defined as

$$\text{total score} = \sum_k \frac{(\text{H}\alpha\ \text{EW}_k - f(t_k))^2}{\sigma^2_{\text{H}\alpha\ \text{EW}_k}}, \tag{B1}$$

where $\text{H}\alpha\ \text{EW}_k$ and t_k are the equivalent width and the age of the excluded k-element, respectively, and f represents the model being tested, so that $f(t_k)$ predicts the value of $\text{H}\alpha$ EW. The model with the lowest score predicts the new data best.

Applying the described cross-validation method with the `scipy` Python package (Virtanen et al. 2020), we found that a first-degree polynomial and a broken power law had the lowest cross-validation scores, indicating that these models can predict the ages based on $\text{H}\alpha$ better. Therefore we confirm the choice of a broken power law to fit the age–activity relation.

ORCID iDs

Rocio Kiman https://orcid.org/0000-0003-2102-3159
Jacqueline K. Faherty https://orcid.org/0000-0001-6251-0573
Kelle L. Cruz https://orcid.org/0000-0002-1821-0650
Jonathan Gagné https://orcid.org/0000-0002-2592-9612
Ruth Angus https://orcid.org/0000-0003-4540-5661
Sarah J. Schmidt https://orcid.org/0000-0002-7224-7702
Andrew W. Mann https://orcid.org/0000-0003-3654-1602
Daniella C. Bardalez Gagliuffi https://orcid.org/0000-0001-8170-7072
Emily Rice https://orcid.org/0000-0002-3252-5886

References

Alonso-Floriano, F. J., Morales, J. C., Caballero, J. A., et al. 2015, A&A, 577, 128
Angus, R., Aigrain, S., Foreman-Mackey, D., & McQuillan, A. 2015, MNRAS, 450, 1787
Angus, R., Morton, T. D., Foreman-Mackey, D., et al. 2019, AJ, 158, 173
Ansdell, M., Gaidos, E., Mann, A. W., et al. 2015, ApJ, 798, 41
Arenou, F., Luri, X., Babusiaux, C., et al. 2018, A&A, 616, A17
Astropy Collaboration, Robitaille, T. P., Tollerud, E. J., et al. 2013, A&A, 558, A33
Baraffe, I., Homeier, D., Allard, F., & Chabrier, G. 2015, A&A, 577, A42
Barnes, S. A. 2003, ApJ, 586, 464
Barnes, S. A. 2007, ApJ, 669, 1167
Barry, D. C. 1988, ApJ, 334, 436
Bayo, A., Barrado, D., Huélamo, N., et al. 2012, A&A, 547, A80
Bell, C. P., Mamajek, E. E., & Naylor, T. 2015, MNRAS, 454, 593
Bell, K. J., Hilton, E. J., Davenport, J. R. A., et al. 2012, PASP, 124, 14
Bergeron, P., Dufour, P., Fontaine, G., et al. 2019, ApJ, 876, 67
Bergeron, P., Wesemael, F., & Beauchamp, A. 1995, PASP, 107, 1047
Bergeron, P., Wesemael, F., Dufour, P., et al. 2011, ApJ, 737, 28
Birky, J., Hogg, D. W., Mann, A. W., & Burgasser, A. 2020, ApJ, 892, 31
Blouin, S., Dufour, P., & Allard, N. F. 2018, ApJ, 863, 184
Bochanski, J. J., Hawley, S. L., Covey, K. R., et al. 2010, AJ, 139, 2679
Bochanski, J. J., Hawley, S. L., Reid, I. N., et al. 2005, AJ, 130, 1871
Bochanski, J. J., Munn, J. A., Hawley, S. L., et al. 2007, AJ, 134, 2418
Bochanski, J. J., Savcheva, A. S., West, A. A., & Hawley, S. L. 2013, AJ, 145, 40
Bodenheimer, P. H. 2011, Principles of Star Formation (Berlin: Springer)
Booth, R. S., Poppenhaeger, K., Watson, C. A., Aguirre, V. S., & Wolk, S. J. 2017, MNRAS, 471, 1012
Bouy, H., & Martín, E. L. 2009, A&A, 504, 981
Boyajian, T. S., Von Braun, K., Van Belle, G., et al. 2012, ApJ, 757, 112
Brandt, T. D., & Huang, C. X. 2015, ApJ, 807, 24
Capitanio, L., Lallement, R., Vergely, J. L., Elyajouri, M., & Monreal-Ibero, A. 2017, A&A, 606, A65
Chabrier, G., & Baraffe, I. 1997, A&A, 327, 1039
Chaplin, W. J., Basu, S., Huber, D., et al. 2014, ApJS, 210, 1
Choi, J., Dotter, A., Conroy, C., et al. 2016, ApJ, 823, 102
Cruz, K. L., & Reid, I. N. 2002, AJ, 123, 2828
Cummings, J. D., Kalirai, J. S., Tremblay, P.-E., Ramirez-Ruiz, E., & Choi, J. 2018, ApJ, 866, 21
Dahm, S. E. 2015, ApJ, 813, 108
Delfosse, X., Forveille, T., Perrier, C., & Mayor, M. 1998, A&A, 331, 581
Dhital, S., West, A. A., Stassun, K. G., Schluns, K. J., & Massey, A. P. 2015, AJ, 150, 57
Dotter, A. 2016, ApJS, 222, 11
Douglas, S. T., Agüeros, M. A., Covey, K. R., et al. 2014, ApJ, 795, 161
Douglas, S. T., Curtis, J. L., Agüeros, M. A., et al. 2019, ApJ, 879, 100
Dressing, C. D., & Charbonneau, D. 2015, ApJ, 807, 45
Eggen, O. J. 1990, PASP, 102, 166
El-Badry, K., & Rix, H.-W. 2018, MNRAS, 480, 4884
Elliott, P., Bayo, A., Melo, C. H. F., et al. 2016, A&A, 590, A13
Fagotto, F., Bressan, A., Bertelli, G., & Chiosi, C. 1994, A&AS, 105, 29
Faherty, J. K., Bochanski, J. J., Gagné, J., et al. 2018, ApJ, 863, 91
Faherty, J. K., Burgasser, A. J., Cruz, K. L., et al. 2009, AJ, 137, 1
Fang, X. S., Zhao, G., Zhao, J. K., & Kumar, Y. B. 2018, MNRAS, 476, 908
Feigelson, E. D., Lawson, W. A., & Garmire, G. P. 2003, ApJ, 599, 1207
Fleming, T. A., Schmitt, J. H. M. M., & Giampapa, M. S. 1995, ApJ, 450, 401
Fontaine, G., Brassard, P., & Bergeron, P. 2001, PASP, 113, 409
Foreman-Mackey, D., Hogg, D. W., Lang, D., & Goodman, J. 2013, PASP, 125, 306
Fouesneau, M., Rix, H.-W., von Hippel, T., Hogg, D. W., & Tian, H. 2018, ApJ, 870, 9
Frasca, A., Guillout, P., Klutsch, A., et al. 2018, A&A, 612, 96
Gagné, J., David, T. J., Mamajek, E. E., et al. 2020, ApJ, 903, 96
Gagné, J., & Faherty, J. K. 2018, ApJ, 862, 138
Gagné, J., Mamajek, E. E., Malo, L., et al. 2018, ApJ, 856, 23
Gaia Collaboration, Brown, A. G. A., Vallenari, A., Prusti, T., & de Bruijne, J. H. J. 2018, A&A, 616, A1
Gaia Collaboration, Prusti, T., de Bruijne, J. H. J., et al. 2016, A&A, 595, A1
Gaidos, E., Mann, A. W., Lépine, S., et al. 2014, MNRAS, 443, 2561
Galli, P. A. B., Joncour, I., & Moraux, E. 2018, MNRAS, 477, L50
Gao, X. H. 2019, MNRAS, 486, 5405
Gennaro, M., Prada Moroni, P. G., & Tognelli, E. 2012, MNRAS, 420, 986
Gentile Fusillo, N. P., Tremblay, P.-E. E., Gänsicke, B. T., et al. 2019, MNRAS, 482, 4570
Gizis, J. E., Monet, D. G., Reid, I. N., et al. 2000, AJ, 120, 1085
Gizis, J. E., & Reid, I. N. 1997, PASP, 109, 849
Gizis, J. E., Reid, I. N., & Hawley, S. L. 2002, AJ, 123, 3356
Goldman, B., Röser, S., Schilbach, E., Moór, A. C., & Henning, T. 2018, ApJ, 868, 32
Gould, A., Bahcall, J. N., & Flynn, C. 1996, ApJ, 465, 759
Haakonsen, C. B., & Rutledge, R. E. 2009, ApJS, 184, 138
Hänninen, J., & Flynn, C. 2002, MNRAS, 337, 731
Hawley, S. L., Gizis, J. E., & Reid, I. N. 1996, AJ, 112, 2799
Holberg, J. B., & Bergeron, P. 2006, AJ, 132, 1221
Hunter, J. D. 2007, CSE, 9, 90
Ivanov, V. D., Vaisanen, P., Kniazev, A. Y., et al. 2015, A&A, 574, 64
Jackson, A. P., Davis, T. A., & Wheatley, P. J. 2012, MNRAS, 422, 2024
Jayawardhana, R., Coffey, J., Scholz, A., Brandeker, A., & van Kerkwijk, M. H. 2006, ApJ, 648, 1206
Jeffers, S. V., Schöfer, P., Lamert, A., et al. 2018, A&A, 614, A76
Jones, D. O., West, A. A., & Foster, J. B. 2011, AJ, 142, 44
Jones, J., White, R. J., Boyajian, T. S., et al. 2015, ApJ, 813, 58
Kenyon, S. J., & Hartmann, L. 1995, ApJS, 101, 117
Kesseli, A. Y., Muirhead, P. S., Mann, A. W., & Mace, G. 2018, AJ, 155, 225
Kiman, R., Schmidt, S. J., Angus, R., et al. 2019, AJ, 157, 231
Kiman, R. 2021, rkiman/M-dwarfs-Age-Activity-Relation: First Release of the Code Used in the Work "Calibration of the Halpha Age–Activity Relation for M Dwarfs," v1.0.0, Zenodo, doi:10.5281/zenodo.4660208
Kiraga, M. 2012, AcA, 62, 67
Kounkel, M., & Covey, K. 2019, AJ, 158, 122
Kowalski, P. M., & Saumon, D. 2006, ApJL, 651, L137
Kraus, A. L., Shkolnik, E. L., Allers, K. N., & Liu, M. C. 2014, AJ, 147, 146
Kraus, A. L., Tucker, R. A., Thompson, M. I., Craine, E. R., & Hillenbrand, L. A. 2011, ApJ, 728, 48
Lallement, R., Capitanio, L., Ruiz-Dern, L., et al. 2018, A&A, 616, A132
Lallement, R., Vergely, J.-L., Valette, B., et al. 2014, A&A, 561, A91
Laughlin, G., Bodenheimer, P., & Adams, F. C. 1997, ApJ, 482, 420
Lawson, W. A., Crause, L. A., Mamajek, E. E., & Feigelson, E. D. 2002, MNRAS, 329, L29
Lee, K. G., Berger, E., & Knapp, G. R. 2010, ApJ, 708, 1482
Lepine, S., Hilton, E. J., Mann, A. W., et al. 2013, AJ, 145, 102
Lépine, S., Rich, R. M., & Shara, M. M. 2003, AJ, 125, 1598
Lépine, S., Thorstensen, J. R., Shara, M. M., & Rich, R. M. 2009, AJ, 137, 4109
Lindegren, L., Hernandez, J., Bombrun, A., et al. 2018, A&A, 616, A2
Lodieu, N., Scholz, R. D., McCaughrean, M. J., et al. 2005, A&A, 440, 1061
López-Santiago, J., Montes, D., Gálvez-Ortiz, M. C., et al. 2010, A&A, 514, 97
Lorenzo-Oliveira, D., de Mello, G. F. P., Schiavon, R. P., Porto De Mello, G. F., & Schiavon, R. P. 2016, A&A, 594, L3
Luhman, K. L., Herrmann, K. A., Mamajek, E. E., Esplin, T. L., & Pecaut, M. J. 2018, AJ, 156, 76
Lyo, A.-R., Lawson, W. A., Feigelson, E. D., & Crause, L. A. 2004, MNRAS, 347, 246
Lyra, W., & De Mello, G. F. 2005, A&A, 431, 329
Malo, L., Artigau, É., Doyon, R., et al. 2014a, ApJ, 788, 81
Malo, L., Doyon, R., Feiden, G. A., et al. 2014b, ApJ, 792, 37
Mamajek, E. E. 2016, A New Candidate Young Stellar Group at d=121 pc Associated with 118 Tauri, Figshare, doi:10.6084/m9.figshare.3122689.v1
Mamajek, E. E., & Hillenbrand, L. A. 2008, ApJ, 687, 1264
Mann, A. W., Dupuy, T., Kraus, A. L., et al. 2019, ApJ, 871, 63
Mann, A. W., Feiden, G. A., Gaidos, E., Boyajian, T. S., & Braun, K. V. 2015, ApJ, 804, 64
Martin, E. L., & Kun, M. 1996, A&AS, 116, 467
Mochnacki, S. W., Gladders, M. D., Thomson, J. R., et al. 2002, AJ, 124, 2868
Mohanty, S., & Basri, G. 2003, ApJ, 583, 451
Mohanty, S., Jayawardhana, R., & Basri, G. 2005, ApJ, 626, 498
Morgan, D. P., West, A. A., Garcés, A., et al. 2012, AJ, 144, 93
Mulders, G. D., Pascucci, I., & Apai, D. 2015, ApJ, 814, 130
Murphy, S. J., & Lawson, W. A. 2015, MNRAS, 447, 1267
Murphy, S. J., Lawson, W. A., & Bessell, M. S. 2010, MNRAS, 406, L50
Ness, M., Hogg, D. W., Rix, H. W., Ho, A. Y., & Zasowski, G. 2015, ApJ, 808, 16
Newton, E. R., Charbonneau, D., Irwin, J., et al. 2014, AJ, 147, 20
Newton, E. R., Irwin, J., Charbonneau, D., et al. 2017, ApJ, 834, 85

Núñez, A., Agüeros, M. A., Covey, K. R., & López-Morales, M. 2016, ApJ, 834, 176
Oh, S., Price-Whelan, A. M., Hogg, D. W., Morton, T. D., & Spergel, D. N. 2017, AJ, 153, 257
Oliphant, T. E. 2006, A Guide to NumPy, Vol. 1 (Spanish Fork, UT: Trelgol Publishing)
Parker, E. N. 1955, ApJ, 122, 293
Paxton, B., Bildsten, L., Dotter, A., et al. 2011, ApJS, 192, 3
Paxton, B., Cantiello, M., Arras, P., et al. 2013, ApJS, 208, 4
Paxton, B., Marchant, P., Schwab, J., et al. 2015, ApJS, 220, 15
Paxton, B., Schwab, J., Bauer, E. B., et al. 2018, ApJS, 234, 34
Pecaut, M. J., & Mamajek, E. E. 2016, MNRAS, 461, 794
Phan-Bao, N., & Bessell, M. S. 2006, A&A, 446, 515
Platais, I., Kozhurina-Platais, V., & van Leeuwen, F. 1998, AJ, 116, 2423
Pöhnl, H., & Paunzen, E. 2010, A&A, 514, 81
Price-Whelan, A. M., Sipőcz, B. M., Günther, H. M., et al. 2018, AJ, 156, 123
Rebull, L. M., Stauffer, J. R., Cody, A. M., et al. 2018, AJ, 155, 196
Reid, I. N., & Cruz, K. L. 2002, AJ, 123, 2806
Reid, I. N., Cruz, K. L., & Allen, P. R. 2007, AJ, 133, 2825
Reid, N., Hawley, S. L., & Mateo, M. 1995, MNRAS, 272, 828
Reiners, A., & Basri, G. 2007, ApJ, 656, 1121
Reiners, A., & Basri, G. 2008, ApJ, 684, 1390
Reiners, A., & Basri, G. 2010, ApJ, 710, 924
Reiners, A., Joshi, N., & Goldman, B. 2012, AJ, 143, 93
Riaz, B., Gizis, J. E., & Harvin, J. 2006, AJ, 132, 866
Ribas, I., Gregg, M. D., Boyajian, T. S., & Bolmont, E. 2017, A&A, 603, A58
Riedel, A. R., Alam, M. K., Rice, E. L., Cruz, K. L., & Henry, T. J. 2017, ApJ, 840, 87
Riedel, A. R., Finch, C. T., Henry, T. J., et al. 2014, AJ, 147, 85
Robertson, P., Endl, M., Cochran, W. D., & Dodson-Robinson, S. E. 2013, ApJ, 764, 3
Rodriguez, D. R., Zuckerman, B., Kastner, J. H., et al. 2014, ApJ, 774, 101
Rodríguez, E., Rodríguez-López, C., López-González, M. J., et al. 2016, MNRAS, 457, 1851
Röser, S., & Schilbach, E. 2020, A&A, 638, A9
Röser, S., Schilbach, E., Piskunov, A. E., Kharchenko, N. V., & Scholz, R.-D. 2011, A&A, 531, A92
Samus', N. N., Kazarovets, E. V., Durlevich, O. V., Kireeva, N. N., & Pastukhova, E. N. 2017, ARep, 61, 80
Schmidt, S. J., Hawley, S. L., West, A. A., et al. 2015, AJ, 149, 158
Schmidt, S. J., Wagoner, E. L., Johnson, J. A., et al. 2016, MNRAS, 460, 2611
Schneider, A. C., & Shkolnik, E. L. 2018, AJ, 155, 122
Schneider, A. C., Shkolnik, E. L., Allers, K. N., et al. 2019, AJ, 157, 234
Shields, A. L., Ballard, S., & Johnson, J. A. 2016, PhR, 663, 1
Shkolnik, E. L., Allers, K. N., Kraus, A. L., Liu, M. C., & Flagg, L. 2017, AJ, 154, 69
Shkolnik, E. L., Liu, M. C., & Reid, I. N. 2009, ApJ, 699, 649
Shkolnik, E. L., Liu, M. C., Reid, I. N., Dupuy, T., & Weinberger, A. J. 2011, ApJ, 727, 6
Silaj, J., & Landstreet, J. D. 2014, A&A, 566, 132
Skinner, J. N., Morgan, D. P., West, A. A., Lépine, S., & Thorstensen, J. R. 2017, AJ, 154, 118
Skumanich, A. 1972, ApJ, 171, 565
Slesnick, C. L., Carpenter, J. M., & Hillenbrand, L. A. 2006, AJ, 131, 3016
Slesnick, C. L., Hillenbrand, L. A., & Carpenter, J. M. 2008, ApJ, 688, 377
Soderblom, D. R. 2010, ARA&A, 48, 581
Soderblom, D. R., Duncan, D. K., & Johnson, D. R. H. 1991, ApJ, 375, 722
Song, I., Zuckerman, B., & Bessell, M. S. 2003, ApJ, 599, 342
Song, I., Zuckerman, B., & Bessell, M. S. 2004, ApJ, 600, 1016
Stauffer, J. R., & Hartmann, L. W. 1986, ApJS, 61, 531
Stauffer, J. R., Hartmann, L. W., Prosser, C. F., et al. 1997, ApJ, 479, 776
Stelzer, B., Marino, A., Micela, G., López-Santiago, J., & Liefke, C. 2013, MNRAS, 431, 2063
Taylor, M. B. 2005, in ASP Conf. Ser. 347, Astronomical Data Analysis Software and Systems XIV, ed. P. Shopbell (San Fransisco, CA: ASP), 29
Terrien, R. C., Mahadevan, S., Deshpande, R., & Bender, C. F. 2015, ApJS, 220, 16
Theissen, C. A., & West, A. A. 2014, ApJ, 794, 146
Tinney, C. G., & Reid, I. N. 1998, MNRAS, 301, 1031
Torres, C. A., Quast, G. R., Da Silva, L., et al. 2006, A&A, 460, 695
Tremblay, P. E., Bergeron, P., & Gianninas, A. 2011, ApJ, 730, 128
Van Der Walt, S., Colbert, S. C., & Varoquaux, G. 2011, CSE, 13, 22
Van Saders, J. L., Ceillier, T., Metcalfe, T. S., et al. 2016, Natur, 529, 181
Virtanen, P., Gommers, R., Oliphant, T. E., et al. 2020, NatMe, 17, 261
Walkowicz, L. M., Hawley, S. L., & West, A. A. 2004, PASP, 116, 1105
West, A. A., Bochanski, J. J., Hawley, S. L., et al. 2006, AJ, 132, 2507
West, A. A., Hawley, S. L., Bochanski, J. J., Covey, K. R., & Burgasser, A. J. 2008a, in Proc. IAU Symp. 258, The Ages of Stars, ed. E. E. Mamajek et al. (Cambridge: Cambridge Univ. Press), 327
West, A. A., Hawley, S. L., Bochanski, J. J., et al. 2008b, AJ, 135, 785
West, A. A., Hawley, S. L., Walkowicz, L. M., et al. 2004, AJ, 128, 426
West, A. A., Morgan, D. P., Bochanski, J. J., et al. 2011, AJ, 141, 97
West, A. A., Weisenburger, K. L., Irwin, J., et al. 2015, ApJ, 812, 3
White, R. J., & Basri, G. 2003, ApJ, 582, 1109
Wielen, R. 1977, A&A, 60, 263
Wilking, B., Gagne, M., & Allen, L. 2008, in Handbook of Star Forming Regions, Vol. II, ed. B. Reipurth (Tucson, AZ: Univ. Arizona Press.), 351
Winters, J. G., Henry, T. J., Jao, W.-C., et al. 2019, AJ, 157, 216
York, D. G., Adelman, J., Anderson, J. E., et al. 2000, AJ, 120, 1579
Zuckerman, B. 2019, ApJ, 870, 27
Zuckerman, B., Bessell, M. S., Song, I., & Kim, S. 2006, ApJL, 649, L115